

# Morphology of low-redshift compact galaxy clusters

## I. Shapes and radial profiles

V. Strazzullo<sup>1\*</sup>, M. Paolillo<sup>1,2,3</sup>, G. Longo<sup>1,3,4</sup>, E. Puddu<sup>4</sup>, S. G. Djorgovski<sup>5</sup>,  
 R. R. De Carvalho<sup>6</sup>, R. R. Gal<sup>7</sup>

<sup>1</sup>Dipartimento di Scienze Fisiche - Università Federico II, Polo delle Scienze e della Tecnologia, via Cinthia, I-80126 Napoli, Italy

<sup>2</sup>Space Telescope Science Institute, 3700 San Martin Dr, Baltimore, MD 21218, USA

<sup>3</sup>Istituto Nazionale di Fisica Nucleare (INFN) - Sezione di Napoli, Italy

<sup>4</sup>Istituto Nazionale di Astrofisica (INAF) - Osservatorio Astronomico di Capodimonte, via Moiariello 16, Napoli, Italy

<sup>5</sup>Palomar Observatory, Mail Stop 105-24, California Institute of Technology, Pasadena, CA 91125, USA

<sup>6</sup>Instituto Nacional de Pesquisas Espaciais - DAS (CEA-NOVO), Av. dos Astronautas 1758, S.J.Campos SP 12227-010, Brazil

<sup>7</sup>Department of Physics, U.C. - Davis, One Shields Ave., Davis, CA 95616, USA

Accepted . Received

### ABSTRACT

The morphology of clusters of galaxies may be described with a set of parameters which contain information about the formation and evolutionary history of these systems. In this paper we present a preliminary study of the morphological parameters of a sample of 28 compact Abell clusters extracted from DPOSS data, measured with a procedure based on the use of the CIAO-Sherpa software, developed at the Center for Astrophysics (CfA) for X-ray data analysis. The morphology of galaxy clusters is parameterized by their apparent ellipticity, position angle of the major axis, centre coordinates, core radius and  $\beta$ -model power law index. Our procedure provides estimates of these parameters (and of the related uncertainties) by simultaneously fitting them all, overcoming some of the difficulties induced by sparse data and low number statistics typical of this kind of analysis. The cluster parameters were fitted in a  $6 \times 6$  Mpc<sup>2</sup> region, measuring the background in a  $4 \text{ Mpc} < R < 5 \text{ Mpc}$  annulus. We also explore the correlations between shape and profile parameters and other cluster properties. Our results can be summarized as follows: one third of this compact cluster sample has core radii smaller than 100 kpc, i.e. near the limit that our data allow us to resolve, possibly consistent with cusped models. The remaining clusters span a broad range of core radii up to  $\sim 1500$  kpc, including some apparently regular clusters with well resolved core radii. More than 80 per cent of this sample has ellipticity higher than 0.2. The alignment between the cluster and the major axis of the dominant galaxy is confirmed at a high significance level, while no correlation is observed with other bright cluster members. No significant correlation is found between cluster richness and ellipticity. Instead, cluster richness is found to correlate, albeit with large scatter, with the cluster core radius. Finally, in contrast with claims in previous works, a flat universe seems to be favoured, and in any case is not excluded, by the power-law index  $\beta$  of our number density profiles.

**Key words:** Galaxies: clusters: general – Galaxies: clusters: individual – observational cosmology

## 1 INTRODUCTION

In CDM cosmological models, the formation of cosmic structures is associated with that of dark matter halos, which form hierarchically from the gravitational collapse of primordial density fluctuations. Unlike galaxies, clusters are dark matter dominated sys-

tems in which the baryons are not radially segregated. Also, unlike galaxies, they form by dissipationless collapse. Thus, clusters in principle provide a more direct probe of the primordial density fluctuations.

The most accurate methods to derive the mass profile of galaxy clusters (and also their internal structure) require either strong/weak lensing analysis or, under the assumption of thermodynamical equilibrium of the system, the velocity dispersion or the X-

\* E-mail: strazzul@na.astro.it (VS); paolillo@na.infn.it (MP)

ray gas density and temperature profiles. Apart from the validity of the equilibrium assumption, the acquisition of the necessary data is often an expensive task for large, statistically significant samples of clusters. Alternatively, under the assumption that galaxies trace the underlying mass distribution, cluster-sized dark halos density profiles can be derived from galaxy number counts. While this method is not exempt from systematic uncertainties, it relies on few assumptions and, unlike the other methods, can be easily applied to large samples of clusters extracted from wide-field surveys.

Navarro, Frenk & White (1996) showed via extensive numerical simulations that in a CDM universe, halos of different mass (from dwarf galaxies to rich clusters) follow a universal cusped profile (hereafter NFW):

$$\frac{\rho}{\rho_{crit}} = \frac{\delta_c}{(r/r_s)(1+r/r_s)^2}. \quad (1)$$

The NFW model and its universality have been challenged by several authors, especially because of the rotation curves of low surface brightness galaxies and dwarf galaxies, which show a relatively flat density distribution (see e.g., Moore et al. 1999; Swaters, Madore & Trewella 2000; de Blok & Bosma 2002). As applied to galaxy clusters, even if the NFW model is often accepted as a good fit to mass density profiles (e.g. Carlberg et al. 1997; Markevitch et al. 1999; Geller, Diaferio & Kurtz 1999; Lewis, Buote & Stocke 2003), controversy still exists and has been recently revived by several authors (see for instance Miralda-Escude 1995; Shapiro & Iliev 2000; Wu & Chiueh 2001; Sand, Treu & Ellis 2002; Biviano & Girardi 2003).

From the number density and luminosity profiles of rich galaxy clusters in the ENACS (ESO Nearby Abell Cluster Survey) catalog, Adami et al. (1998, 2001, hereafter AMKB98, AMUS01) found that, if the faint cluster members are included, a core model of the form:

$$s(r) = s_0 \left( \frac{1}{1 + (r/r_{core})^2} \right)^\beta \quad (2)$$

reproduces the galaxy number density profiles more accurately than cusped (NFW-like) models; the trend turned out to be even more evident for luminosity profiles. This result is in agreement with models predicting different evolutionary scenarios for the luminous and the faint populations of galaxies in clusters. In fact, AMUS01 suggested that galaxy number density and luminosity profiles could be originally cusped, as expected from simulations of dark matter halos (Navarro, Frenk & White 1996, 1997) and that, afterward, the cusp in the number density profile could be erased by merging events. This would produce a cusp in the bright galaxy luminosity profile, as well as the core observed in the faint galaxy luminosity profile through tidal disruption of small galaxies near the cluster centre.

The cluster morphological parameters thus bear relevant information on the cluster dynamical status and formation scenarios. For instance, the core radius  $r_{core}$  is a characteristic scale-length of the galaxy distribution inside the cluster, and it has been shown to be tightly correlated with the virial radius (see Girardi et al. 1995, hereafter G95). Other relevant information may be obtained from the cluster shapes once they are approximated as spheroids. Rich clusters have been found to show ellipticities up to 0.8, with a mean value of 0.4, and a correlation between ellipticity and richness (the richer the cluster, the more spherical the shape – e.g. Struble & Ftaclas 1994; de Theije, Katgert & van Kampen 1995). Moreover, the cluster shape distribution is directly connected to the cosmological parameters: a low density universe produces more

concentrated, spherically symmetric clusters than a  $\Omega = 1$  scenario (e.g. Evrard et al. 1993).

In this work we present a preliminary study of the morphological properties of a sample of 28 nearby compact Abell clusters extracted from the Digitized Palomar Sky Survey (DPOSS) (Djorgovski et al. 1999). The advantages of using DPOSS data are mainly in the wide sky coverage (which allows an extended region around each cluster to be studied), the homogeneous photometric system of the whole data set, and good control of the catalogue completeness and selection criteria (Weir et al. 1995; Paolillo et al. 2001).

We point out that we do not attempt to test which model best describes the actual cluster profile. Instead, we adopt the beta model as a statistically adequate, analytically convenient description of the galaxy distribution and investigate the correlations between shape, profile parameters and other cluster properties. The comparison between different cluster profile models requires careful stacking of individual clusters to obtain a sufficient S/N ratio (see for instance Carlberg, Yee & Ellingson 1997; de Theije & Katgert 1999), and is beyond the purpose of this work.

The paper is structured as follows: in section § 2 we describe the data and the cluster sample, in section § 3 we describe the method used to model cluster radial profiles and to derive morphological parameters, while in sections § 4 and § 5 we present our results and summarize our conclusions. Throughout this paper we use  $H_0 = 50$ ,  $\Omega_M = 1$ ,  $\Omega_\Lambda = 0$ . We do not adopt the usual concordance cosmology in order to simplify the comparison with Paolillo et al. (2001), on which this work is partially based. Cosmological parameters only affect our results via the conversion from angular to linear distances. Using a  $H_0 = 70$ ,  $\Omega_\Lambda = 0.7$ ,  $\Omega_M = 0.3$  cosmology, distances would be smaller by approximately 20-25 % in our redshift range.

## 2 DATA AND CLUSTER SAMPLE SELECTION

This work is based on catalogues produced from DPOSS data (Djorgovski et al. 1999) with the SKICAT package (Weir et al. 1995). We started with the initial sample of 80 Abell clusters described in Piranomonte et al. (2001), which had available calibration frames and at least one reliable spectroscopic redshift (see Paolillo et al. 2001) at the beginning of this work. We note that a much larger cluster sample extracted from DPOSS catalogs is currently available and its analysis is postponed to a future work (Gal et al. 2003).

The photometric completeness limit was estimated for each cluster and in each band independently; typical values are  $m_r \simeq 20$  and  $m_g \simeq 20.5$  in the Gunn-Thuan photometric system (Paolillo et al. 2001; Paolillo et al., in preparation); K-corrections were not taken into account since, due to the small redshift range covered by the clusters in our sample ( $z < 0.27$ , with only 2 clusters at  $z > 0.2$ ), they are negligible; furthermore, the lack of morphological information for the individual galaxies would introduce unnecessary ambiguities.

For each cluster we extracted from the SKICAT catalogues all objects brighter than  $m_g = 20$  contained within a square region of  $10 \times 10 \text{ Mpc}^2$  centered on the cluster centre (as listed in the Abell catalogue), detected in both the g and the r bands (the i-band was not used since it is much shallower than the others) and classified as galaxies in both filters. The large region around each cluster ( $10 \times 10 \text{ Mpc}^2$ ) was selected in order to sample the cluster galaxy distribution out to a significant distance from the cluster centre (1 Abell

radius = 3 Mpc with our cosmology), and to have a control field around each cluster wide enough to achieve a proper background determination. As discussed later (§ 3.1), the proper cluster fitting was performed on a smaller region ( $6 \times 6$  Mpc).

Galaxy clusters may exhibit different degrees of internal subclustering (Baier 1979; Geller & Beers 1982; West, Oemler & Dekel 1988; Dressler & Schechtman 1988; Bird 1994; Pinkney et al. 1996; Solanes, Salvador-Solè & González-Casado 1999; Knebe & Müller 2000). In particular, cluster substructure may generally be divided into four categories: dynamical subclumps residing in generally relaxed systems; young clusters in an early merging state; dynamically bound units in the cluster outskirts; and chance projections of groups. Discriminating between these four different cases is extremely difficult in the absence of velocity information. Moreover, subclustering at large distances from the cluster centre ( $> 1$  Mpc) may often be due to fluctuations in the extended host supercluster (West & Bothun 1990).

Obviously, the presence of substructures would make the modeling of the radial profile almost meaningless, since there would be no radial symmetry nor a well defined core radius associated with a central relaxed region of the system. For the purpose of this work, we excluded from our sample all clusters with obvious large substructures by visually inspecting the galaxy surface density maps (smoothed with a Gaussian filter with  $\sigma = 250$  kpc) and rejecting those with multiple isolated peaks within 3 Mpc of the cluster center (see figure 1).

While this is an empirical criterion, a more objective method is not straightforward in our case, due to the low number of galaxies and the lack of spectroscopic information. Our criterion allows the selection of clusters that are broadly regular and single peaked on large scale, and therefore our sample includes several examples of regular clusters like A1914, A1835, A566 (Buote & Tsai 1996; Majerowicz, Neumann & Reiprich 2002; Zhou et al. 2003). However, we also have some systems which are not truly relaxed, generally known from X-ray or dynamical analysis such as the disturbed morphology of A2061 (Postman, Geller & Huchra 1988), the late merger A2142 (Buote & Tsai 1996), and the bimodal cluster A98 (Beers, Geller & Huchra 1982; Krempeck-Krygier & Krygier 1995). We prefer to use a homogeneous criterion for the whole sample without discarding individual clusters for which additional data are available, even if this means that we have to accept some degree of ‘imperfection’, e.g. low density tails or some level of substructure in the cluster core.

It may be argued that a smaller smoothing scale may reveal smaller scale substructures. In figure 2 we show the comparison of density maps smoothed with 250 kpc and 150 kpc smoothing scales for two representative cases. We find that, using a 150 kpc scale, only five clusters (A175, A655, A910, A1661, A2177) reveal significant substructure that may in principle question their inclusion in the sample. Our data do not allow to study smaller scale structures in the cluster core since the distance between galaxies is on average greater than 50 kpc (i.e. on scales smaller than 150 kpc shot noise dominates the galaxy distribution). Note however that a smaller smoothing window only affects the sample selection and not the actual fitting (see section § 3.1).

The final sample of clusters which will be the subject of the following analysis consists of 28 objects listed in table 1.

### 3 THE DETERMINATION OF RADIAL PROFILES

#### 3.1 Model and statistics

Modeling the 2D distribution of galaxies in clusters is a problematic task due to the small number statistics which affects these sparse data. The classical approach which obtains the number count radial profile by binning and counting galaxies in concentric circular shells, results in the loss of relevant morphological information. Moreover, because of contamination from background/foreground objects, there is a significant decrease in the S/N ratio of the resulting profiles.

Maximum likelihood methods as initially proposed by Sarazin (1980), applied directly to the galaxy positions without any binning, allow these problems to be partially overcome. In general, these methods rely on three fundamental assumptions: i) the observed positions of galaxies are statistically independent (i.e. no substructure is present); ii) the local background is assumed to be uniform; iii) the shape of the galaxy number density function is assumed to be known and characterized by a small number of parameters.

In the literature, radial profiles of galaxy clusters have mainly been determined by means of different implementations of this method. However, even if in principle it would be possible to fit all the parameters simultaneously, in practice the minimization often has to be accomplished in steps, fitting the shape (centre coordinates, ellipticity and position angle) and the profile (core radius, power law index etc.) parameters separately (e.g. AMKB98; see also G95, AMUS01 and Girardi & Mezzetti 2001). Furthermore, in such cases the strong correlation between the model parameters may produce spurious results.

Taking advantage of the formal analogies existing between X-ray data (photon hit positions and photon energies) and galaxy catalogues (galaxy positions and magnitudes) in terms of sparse distribution and low statistics, we tailored to our specific needs the Sherpa package present in the CIAO<sup>1</sup> software, developed at the Chandra X-ray Center. Our procedure allows us to fit all the parameters of the galaxy distribution at the same time, instead of requiring a multi-step approach.

The Sherpa software works on binned data. To minimize the loss of information, we binned the galaxy positions using a square grid of bin size 50 kpc, in order to have at most one galaxy per bin, except for a few clusters in which the highest density bin may contain two galaxies. This is in principle equivalent to using unbinned data.

We assume that galaxy clusters can be described by a standard two dimensional  $\beta$ -model of the form:

$$f(r) = f(x, y) = \frac{\Sigma_0}{(1 + (r/r_{core})^2)^\beta} \quad (3)$$

where:

$$r(x, y) = \frac{\sqrt{\bar{x}^2(1 - \epsilon)^2 + \bar{y}^2}}{1 - \epsilon} \quad (4)$$

$$\bar{x} = (x - x_0) \cos \theta + (y - y_0) \sin \theta \quad (5)$$

$$\bar{y} = (y - y_0) \cos \theta - (x - x_0) \sin \theta. \quad (6)$$

This implies that the characterization of the galaxy profile of each cluster requires the simultaneous fit of the following parameters:

<sup>1</sup> We used CIAO version 2.2.1. Full documentation can be found at <http://cxc.harvard.edu/ciao/>

- i) shape parameters: centre coordinates  $(x_0, y_0)$ , ellipticity  $\epsilon$ , and position angle  $\theta$ ;
- ii) profile parameters: core radius  $r_{core}$ , power law index  $\beta$ , central density  $\Sigma_0$  at  $x_0, y_0$ , and local background density  $\Sigma_{bkg}$  (assumed to be uniform)<sup>2</sup>.

As already explained in the introduction, our goal is not to determine which function describes best the profile of galaxy clusters. We are heavily limited by the small number of galaxies and by the sparse nature of the galaxy distribution, which makes it difficult to discriminate between different profiles for most clusters in our sample. As an example, in figure 3 we compare the best-fit NFW and  $\beta$ -model profiles, derived through an azimuthally averaged unidimensional fit on binned data, for A286. Even with this simplistic procedure, which minimizes the number of fitted parameters, the two models are almost indistinguishable. In § 4 we will discuss further the possibility that our clusters follow a cusped distribution.

The use of parametric methods has also been criticized, in particular when not dealing with truly sparse data or theoretically well-established functional forms. This criticism arises mainly from the fact that projection effects can transform two intrinsically different spatial profiles to very similar projected profiles, and by the application of parametric methods to a typical case of an ill-conditioned problem such as the radial profile estimation (Merritt & Tremblay 1994). Although in our case we are actually dealing with sparse data, so that a non-parametric approach would be quite difficult, we are aware that we are simply using a statistically convenient empirical formula in a consistent manner.

In performing our fit we used a maximum likelihood approach, where the likelihood function is the product of the individual probabilities  $P_i$  computed for each bin  $i$  assuming that galaxy counts are sampled from a Poisson distribution:

$$\mathcal{L} = \prod_i \frac{P_i^{N_i}}{N_i!} \exp(-P_i). \quad (7)$$

In equation (7)  $P_i$  is the sum of cluster and background model amplitudes, and  $N_i$  is the number of observed galaxy counts in bin  $i$ . The Cash statistic (Cash 1979):

$$C = 2 \left[ \sum_i P_i - N_{i,S} \ln P_i \right] \quad (8)$$

is derived from the likelihood function by taking the logarithm of  $-\mathcal{L}$  and dropping the factorial term, which is constant in fits to the same dataset. Unlike the more traditional  $\Delta\chi^2$ , the Cash statistic may be used regardless of the number of counts in each bin (for details, see the Sherpa Reference Manual 2001). We note that, with poorly sample data, the Cash statistic works better than a  $\chi^2$  statistic, even if the latter is tailored to work with low number counts.

### 3.2 Fitting procedure and validation

The application of the CIAO-Sherpa software for the determination of cluster radial profiles was extensively tested on real and simulated data. A first problem to solve was how to estimate the galaxy background. Tests performed on the  $10 \times 10 \text{ Mpc}^2$  region (i.e.

<sup>2</sup> The external constraint due to the normalization of the model to the observed total number of galaxies, reduces the degrees of freedom of the problem. Therefore, only three of the four profile parameters are actually independent.

$R \lesssim 5 \text{ Mpc}$ ) showed that, for the majority of clusters, the fit was able to recover within 10% the estimate of the background level as obtained manually, by measuring the average galaxy counts in an external annulus ( $4 \text{ Mpc} < R < 5 \text{ Mpc}$ ) around the cluster. Both the manual and fitted estimate are reported in table 3.

For low S/N objects, while still retrieving the correct background, problems were encountered in fitting the other cluster parameters in the whole  $10 \times 10 \text{ Mpc}^2$  region. This is a natural consequence of the fact that with low S/N objects, the background fluctuations undermine the cluster detection itself. Therefore, in order to be consistent, we decided to fix for all the clusters the background density to the value measured in the  $4 < R < 5 \text{ Mpc}$  annulus, and to fit the cluster in a smaller region of  $6 \times 6 \text{ Mpc}^2$ . We tested the effect of a background under- or over-estimation by 15% ( $\simeq 2\sigma$  upper limit on the background fluctuations measured in our catalogs over a  $6 \times 6 \text{ Mpc}^2$  window) of its measured value on the fitted parameters  $r_{core}$ ,  $\beta$ , ellipticity and position angle: as expected, the ellipticity and position angle are scarcely affected, while there is a systematic effect on  $\beta$  and, to a lesser extent, on the core radius (see figure 4).

The  $6 \times 6 \text{ Mpc}^2$  was adopted as an optimal compromise between the requirement to sample a relevant part of the cluster, possibly out to the radius where the galaxy density approaches the background level, and the attempt to maximize the S/N ratio of our galaxy counts. Note that this region corresponds to a radius  $R = 3 \text{ Mpc}$ , i.e. one Abell radius in our adopted cosmology, and approximately to the median cluster virial radius (Carlberg, Yee & Ellingson 1997). Furthermore this choice helps to prevent strong background fluctuations or nearby ( $3 < R < 5 \text{ Mpc}$ ) overdensities from affecting the cluster parameter evaluation. The  $4 \text{ Mpc} < R < 5 \text{ Mpc}$  annulus represents a region distant enough not to be contaminated by the cluster itself while sufficiently nearby to be representative of the local cluster background. Since the use of a  $6 \times 6 \text{ Mpc}$  region may include small local substructures (either due to the cluster or the background) which are not discarded by our sample selection criteria, we performed an additional fit on a smaller  $3 \times 3 \text{ Mpc}^2$  area. The results, which are discussed in section § 4, show that the fits performed on the smaller region, while severely affected by the lower statistics, are basically consistent with those performed over the  $6 \times 6 \text{ Mpc}^2$  area. We show the dependence of the retrieved parameters on the size of the fitted region in figure 5. The estimates in the three different regions appear consistent within the errors in the vast majority of cases. The  $\beta$  parameter shows indeed a large scatter, as this is the less stable of the fitted parameters, due to low S/N and incomplete profile sampling in small apertures.

The fit results do not depend on the bin size, provided that the bin is small enough to avoid any loss of information (i.e.  $\sim 1$  galaxy  $\text{bin}^{-1}$ ). Furthermore, the shape parameters (centre coordinates,  $\epsilon$  and  $\theta$ ) derived from the fit are consistent within the errors with respect to profile ( $r_{core}, \beta$ ) parameter variations (see figure 5).

We don't find any significant correlation of the fit result on the starting values: using different values within the permitted range (i.e. [0:3000] kpc for  $r_{core}$ , [0:4] for  $\beta$ , [0:1] for  $\epsilon$ , and [0:2 $\pi$ ] for  $\theta$ ), the difference in the retrieved output is 5–20% for  $r_{core}$ , 1–15% for  $\beta$ , less than 2% for  $\epsilon$ , and less than 0.1% for  $\theta$  (the larger differences quoted for  $r_{core}$  and  $\beta$  occurring for the clusters with very large core radius).

Finally, we tested our procedure on a sample of 230 mock clusters. Mock clusters are generated following a  $\beta$ -model profile, and all clusters are produced with centre coordinates in the centre of the mock catalog region, which in pixel units is  $(x_0, y_0) = (60, 60)$ ,

ellipticity = 0.4 and  $\beta$  = 0.8, representative of typical values in the real sample, and position angle = 1. The core radius, central density and background density are randomly chosen in such a way that the total number of objects, the background density  $\sigma_{bkg}$ , the cluster core radius, and the S/N reflect those of the real clusters. The fit on the mock catalogs is performed exactly in the same way as for real clusters: background density is fixed and all the other parameters are left free to float.

The mean ellipticity retrieved is  $0.33 \pm 0.16$ , the mean  $\beta$  is  $0.83 \pm 0.26$ , the mean centre coordinates are  $(60.2, 60.1) \pm (1.2, 1.5)$ , the mean position angle is  $1.3 \pm 0.7$ . The distributions of the retrieved ellipticity,  $\beta$ , centre coordinates and position angle are shown in figure 6, and are to be compared with the above reported true-values of  $(x_0, y_0) = (60, 60)$ , ellipticity = 0.4, position angle = 1., and  $\beta$  = 0.8. In figure 7 we show the retrieved vs. true core radius. These plots show that our fitting procedure yields reliable results without significant systematic effects, except possibly for the ellipticity which is slightly skewed toward lower values. This is a result of the background contribution which tends to azimuthally smooth the galaxy distribution. This effect however does not affect our results, as discussed in § 4. The large dispersion in the P.A. distribution is mainly due to low S/N. In fact, additional simulations with very high S/N mock clusters show that for  $\epsilon > 0.3$  the position angle is correctly retrieved within 10 degrees at most. Note that while the core radius exhibits a large relative dispersion at small radii, due to the difficulty of obtaining a reliable estimate of  $r_{core}$  for small core radii (due to the low S/N within  $r_{core}$ ), the retrieved value is in most cases representative of the true value, and the scatter found for mock clusters is consistent with the average measurement errors that we derive for the real sample.

### 3.3 Fitting results

Summarizing the discussion in section § 3.2, we performed the fit for all clusters in a  $6 \times 6 \text{ Mpc}^2$  square region, with a bin size of 50 kpc and with the background density fixed to the value measured for each cluster in an external annulus ( $4 \text{ Mpc} < R < 5 \text{ Mpc}$ ). Note that the use of the same physical area ( $6 \times 6 \text{ Mpc}^2$ ) for all clusters implies that we are considering a different density threshold for each cluster. However, this does not affect our results since we sample the cluster out to a radius where the S/N is negligible, while the use of a fixed density threshold would introduce other effects, such as a dependence on the background fluctuations.

The resulting parameters are listed in table 2. Error estimates are calculated by leaving only the highly correlated parameters free to vary (i.e.  $\epsilon - \theta$  and  $r_{core} - \beta - \Sigma_0$ ), and fixing all the others. Even if these are not the formally correct errors, they provide a meaningful uncertainty on the parameter estimates. The formal errors (where all the fit parameters are left free to vary) would often be unconstrained, given the low counts and the large number of parameters being fit.

As a template case, we show in figure 8 the results of the fitting procedure for the cluster A98. In the upper left panel, the solid line traces the best-fit profile and the dots show the measured density profile. The data and the model are binned using the same set of annuli centered on the cluster centre defined by the fit. We point out that this binning is only used for visualization purposes and it is not involved in the determination of the best-fit parameters. In the upper right panel, we plot the cluster isodensity contours against the model.

In the lower left and middle panels, we plot the confidence contours at  $1\sigma$  and  $2\sigma$  for the highly correlated parameters, namely

$\epsilon - \theta$  and  $r_{core} - \beta$  (with  $\Sigma_0$  free to vary). Finally, in the lower right panel we plot the distribution of  $|\cos(\theta_{galaxies} - \theta_{cluster})|$  (solid line) and the expected histogram for a random distribution of the galaxy position angles (dashed line). For the other clusters in the sample we show only the three most significant plots, namely the cluster isodensity contours against the model, the fitted profile, and the  $|\cos(\theta_{galaxies} - \theta_{cluster})|$  distribution (fig. 9).

## 4 DISCUSSION

In figure 10 we present the distribution of ellipticities (left panel), slopes  $\beta$  (middle panel), and core radii (right panel) derived from our fits. Even though the sample was selected to include clusters with an overall regular morphology, we find a wide range of ellipticities, with mean value  $\bar{\epsilon} = 0.47$  and dispersion  $\sigma_\epsilon = 0.2$ ; note that, given the systematic error measured by our simulations (§ 3.2), the real ellipticity distribution is expected to be slightly skewed toward larger elongations by  $\Delta\epsilon \sim 0.07$ . While this result is in fair agreement with the  $\epsilon$  distribution measured by de Theije, Katgert & van Kampen (1995), it is in contrast with AMKB98, who found on average low ellipticities, consistent with  $\epsilon \simeq 0$ . However, AMKB98 and AMUS01 were mostly interested in the central cluster region, in order to compare cusped and core profiles; as these authors point out, their study is limited to the very central region of the cluster ( $\simeq 500$  kpc) specifically chosen to avoid substructures. This implies that, apart from possible aperture biases which could affect the result, the cluster region that they fit has intrinsically very small ellipticity.

In fact, in our sample six out of the eight less regular clusters mentioned in § 2 have ellipticity above the mean.

As noted in section § 3.2, in order to better evaluate possible effects introduced by overlooked background substructures in the cluster outskirts, we performed an additional fit over a smaller  $3 \times 3 \text{ Mpc}^2$  region. While the parameters derived in this way are more uncertain because of the lower statistics, and possibly biased by the exclusion of the cluster external region, the ellipticity distribution and the presence of the peak at  $\epsilon \simeq 0.5$  are confirmed also using the parameters derived from this smaller region (the dashed line in figure 10). Furthermore, in figure 11 we plot the position angles  $\theta$  derived within the  $6 \times 6 \text{ Mpc}^2$  region against those derived within the  $3 \times 3 \text{ Mpc}^2$  region (clusters A2061, A2083, A2178 and A910 are not included because no reliable parameters could be determined for them in the  $3 \times 3 \text{ Mpc}^2$  region). The two estimates are fully consistent and the few points scattered above and below the line are clusters with  $\epsilon \leq 0.25$ , i.e. objects for which the error on the position angle is systematically larger (the higher the ellipticity, the better constrained the position angle of the major axis). This result shows that there is no significant substructure in the cluster outskirts which would affect the cluster P.A., even though the contribution of cluster galaxies is non-negligible between 1.5 and 3 Mpc from the cluster centre: a significant fraction (between 20 and 60 per cent, with a median value of approximately 50 per cent) of cluster members is found in this external region. Therefore, any study of cluster structure sampling less than  $1.5 \text{ h}^{-1} \text{ Mpc}$  in radius is missing a significant cluster contribution.

The power-law slope  $\beta$  has a peak at  $\sim 0.7$ , with  $\bar{\beta} = 0.8$  and dispersion  $\sigma_\beta = 0.27$ ; both the average value and the shape of the distribution are in very good agreement with the results obtained by Popesso et al. (2004) based on the ROSAT-SDSS galaxy cluster sample, as well as with the results of Girardi & Mezzetti (2001) based on a sample of moderate/high redshift clusters. On the other

hand, our results are again in contrast with those of AMKB98, who found  $\beta = 1.02 \pm 0.08$  for their sample of 60 clusters. Even though our distribution is quite broad, the average value of  $\bar{\beta}$  is inconsistent at the  $> 3\sigma$  level<sup>3</sup> and none of the clusters in the AMKB98 sample has  $\beta < 0.84$ . While our catalogues are somewhat deeper ( $\sim 0.5$  mag) than the ones used by AMKB98, the main differences between us and AMKB98 are that the latter sample a smaller region, thus excluding the contribution of the cluster outskirts, and by the different approach used to estimate the background. Note however, that the fits performed on our smaller  $3 \times 3$  Mpc region, which is closer to the AMKB98 area ( $r > 5r_{core} \sim 1000$  kpc<sup>4</sup>), still yield  $\bar{\beta} = 0.75$ . The two  $\beta$  estimates for the individual clusters are consistent within the errors and there is no evident correlation of  $\beta$  with the size of the sampled region. Note that, according to figure 10 of AMKB98 (based on simulations by Crone & Evrard 1994; Jing et al. 1995; Navarro, Frenk & White 1995; Walter & Klypin 1996) our  $\beta$  distribution is compatible with flat universe models either with zero (standard CDM) or non-zero cosmological constant ( $\Omega_m = 0.2 \div 0.3$  and  $\Lambda = 0.7 \div 0.8$ ), in contrast to the AMKB98 result which favoured an open cosmology. We remind, however, that the validity of cosmological constraints obtained through this method is still debated, and depends on the used simulations.

The median core radius is  $r_{core} = 310$  kpc, but the distribution is strongly skewed toward low values with a marked peak at  $r_{core} \sim 100$  kpc. Approximately 1/3 of our sample has  $r_{core} < 100$  kpc, corresponding to 2 pixels in our fitted maps; for such clusters  $r_{core}$  is thus only marginally resolved, as discussed in § 3.1, so that we cannot exclude a cusped profile. On the other hand 7 clusters have core radii greater than 500 kpc; among these we find six of the less regular systems discussed in § 2.

Some correlation between the dynamical state of the cluster and its core radius is clearly expected, and in fact the most regular clusters (i.e. A79, A763, A971, A1677, A2065, A2083, A2223) all have very small core radius. The intermediate values of core radii refer to clusters which are generally single peaked, but exhibit some broader asymmetric overdensity region, or a filamentary structure. These systems also include the examples of known regular clusters mentioned in § 2.

Our core radii, including the whole sample, are on average larger than those measured by AMKB98 and AMUS01. However, our mean core radius excluding the eight less regular systems would be 213 kpc, with a median of 140 kpc. Nonetheless, AMKB98 found only 6 clusters out of 60 with  $r_{core} < 100$  kpc. Thus our sample spans a broader range of core radii (mostly due to the inclusion of less regular systems) but is also more peaked toward low values. This could be due to intrinsic differences in the nature of the cluster sample (indeed Solanes, Salvador-Solé & González-Casado 1999 found a very low level of substructure in the ENACS clusters), as well as to the different area used, and possibly to differences in the method adopted, as the intrinsic coupling between  $r_{core}$  and  $\beta$  in the model (we show for reference the  $r_{core}$  vs.  $\beta$  relation in figure 12) is expected to produce larger core radii in correspondence of the steeper power-law slopes.

On the other hand, the peak of the core radii distribution at 100 kpc is consistent with the small values ( $< 100h^{-1}$  kpc) of the core

<sup>3</sup> The error on  $\bar{\beta}$  is  $\sigma_\beta/\sqrt{N}$  where  $N$  is the number of clusters in the sample.

<sup>4</sup> We rescaled the AMKB98 sizes by a factor 2 since they assume a cosmology with  $H_0 = 100$ ,  $q_0 = 0$

radius recently reported by several authors (e.g. Girardi & Mezzetti 2001; Katgert, Biviano & Mazure 2004). Our tests (cfr. figure 4) show that a systematic underestimate of our background level by  $\simeq 15\%$  (or viceversa an overestimate of AMKB98) would result in an average  $r_{core}$  consistent with the AMKB98 value, provided that the most irregular clusters discussed in § 2 are excluded from the sample. However the  $\beta$  distribution remains inconsistent at the  $3\sigma$  level.

The fits performed on the  $3 \times 3$  Mpc region are generally consistent with those performed on the whole  $6 \times 6$  Mpc area, even though somewhat smaller, yielding a median  $r_{core} = 220$  kpc. However a KS test still rejects the hypothesis that our  $3 \times 3$  Mpc sample and the AMKB98 one are drawn from the same distribution at the 97% level. Note that a misplacement of the cluster center would flatten the central density profile resulting in larger core radii (see for instance Beers & Tonry 1986). According to AMKB98, displacements smaller than 100 kpc have very small effect on the central profile even in the extreme case of a cusped distribution. Thus while such an effect could explain the few clusters with very large  $r_{core}$ , it is unlikely to affect the majority of the clusters.

Significant alignment between clusters and their dominant galaxies has often been observed (see Lambas, Groth & Peebles 1988, and references therein). This effect seems to be independent of cluster richness (Fuller, West & Bridges 1999) and is confirmed up to high redshift. It involves only the cluster dominant galaxy, while the other bright galaxies appear to be randomly oriented, so that the alignment has been claimed to be produced by the same processes that created the dominant galaxy (Kim et al. 2001). In figure 13 we show the misalignment between the position angles of the clusters and those of their brightest cluster members (BCM), for those clusters with ellipticity large enough for the position angle to be well constrained. We note that the BCM definition itself depends on the observed area and that it may happen that the BCM lies far from the cluster centre, thus questioning the association of the galaxy with the cluster (if no redshift measurement is available). Because of this reason, when the BCM was located in the cluster outskirts we used the position angle of the giant elliptical closer to the actual cluster centre, as derived from the fitting procedure. In our case, however, this correction affects only slightly the alignment results, since it involves less than one third of the ‘high ellipticity sample’ (i.e.  $\epsilon > 0.25$ ). As can be seen, the correlation existing between the two quantities is confirmed: the random distribution is rejected at a significance level higher than 99.9 %.

For the other galaxies in the cluster, inspection of the right panels in figure 9 shows that the distribution of their position angles relative to the cluster orientation are consistent with a random distribution, with the possible exception of clusters A2065, A2142, A2178 and A2223. In fact, according to the Kolmogorov-Smirnov confidence levels listed in table 3 (column 9), these four clusters show a position angle distribution significantly different from the random case.

To compare the morphological parameters with the cluster richness we considered two different estimates. The first ( $R_A$ ) is calculated using a criterion similar to the Abell definition, counting how many galaxies fall in the cluster area, with magnitudes in the range  $[m_3, m_3 + 2]$ , and then subtracting the number of field galaxies in the same magnitude range and in an equally large region. The Abell richness estimate, while being historically and operationally correct, is known to suffer from several drawbacks, mostly due to the use of a fixed apparent magnitude range (see, for instance Gal et al. 2003).

For these reasons we also use a second richness estimate  $R_{LF}$

based on the cluster luminosity function, which allows us to exploit the entire galaxy sample down to the completeness limit. We used the luminosity functions (LFs) derived by Paolillo et al. (2001; Paolillo et al., in preparation) to compute, for each cluster, the ratio of the number of galaxies brighter than its absolute completeness limit to the number of galaxies brighter than the same limit in the deepest sampled cluster (Garilli, Maccagni & Andreon 1999). Assuming that the luminosity function has a universal shape, this ratio provides an estimate of the richness of each cluster relative to the richness of the deepest sampled one. While  $R_{LF}$  is not exempt from uncertainties, in particular due to the assumption of the universality of the luminosity function (which is challenged by recent data, e.g. Piranomonte et al. 2001, Paolillo et al. in preparation), we note that this approach is equivalent to the use of a fixed absolute magnitude range, and in fact  $R_{LF}$  is well correlated to the richness estimate based on  $M^*$  employed by Gal et al. (2003). A comparison between  $R_A$  and  $R_{LF}$  is shown in Figure 14.

In Figure 15 we show the dependence of the cluster core radius on the cluster richness. While the core radius shows little dependence on the Abell richness, a mild correlation (correlation coefficient of 0.62) is found using the LF richness estimate. The stronger correlation found with  $R_{LF}$  could be due to the fact that the latter quantity is a better estimator of the cluster richness since it takes into account the entire detected galaxy population, i.e. the same population used to measure the morphological parameters, while  $R_{Abell}$  samples only the brightest galaxy members. Furthermore, if the core is mainly produced by the fainter galaxies, as suggested by AMUS01, we expect a better correlation with  $R_{LF}$  than with  $R_{Abell}$ . This could also explain the lack of correlation found by G95, who used the Abell richness.

The better reliability of the richness  $R_{LF}$  could also be supported by the mild correlation of the cluster X-ray luminosity with  $R_{LF}$  (correlation coefficient 0.6), even with only 21 clusters for which X-ray luminosities are available, while no evident correlation can be seen with the Abell richness (see figure 17).

Finally, we checked for correlations between the ellipticity and the cluster richness, as found for instance by de Theije et al. (1995). In figure 16 we plot the ellipticity-richness relation for both  $R_{LF}$  and  $R_A$ ; empty symbols mark the less regular clusters discussed earlier, that are expected to show a larger ellipticity. We do not find any significant correlation between the ellipticity and the cluster richness. We note however that clusters with  $R_A < 40$  tend to reach higher ellipticities, while no cluster with  $\epsilon > 0.6$  is found at larger richesses. Thus we cannot exclude that richer clusters tend to have, on average, smaller ellipticities. A larger sample is required to confirm this trend.

No evident correlation can be seen between the cluster morphological parameters and the cluster X-ray luminosity; however, X-ray luminosities are available for only 21 clusters of this sample, and the errors on the derived morphological parameters are large, thus this work is not suitable to study such correlations.

## 5 CONCLUSIONS

As already stressed by many authors (see, for instance, G95), the derivation of cluster's morphological parameters is strongly dependent on the properties of the galaxy sample. In particular, inhomogeneity of data (in terms of photometric bands, limiting magnitudes, etc.), and incomplete coverage of the cluster area, may introduce systematic errors in the derived sizes, richesses, ellipticities, etc. In order to minimize these problems, our sample was derived

from a homogeneous data set extracted from DPOSS data with well controlled photometric errors, limiting magnitudes, and wide area coverage. The sample was cleaned of all objects with visually evident signs of substructure, in an attempt to fit only compact clusters for which meaningful values of the profile parameters could be derived. The morphological parameters, namely the core radius,  $\beta$  power law index, ellipticity, position angle, and richness were derived, using software originally designed for X-ray data analysis, from the unsmoothed and essentially unbinned galaxy distributions.

The most relevant results of this work may be summarized as follows:

- One third of the clusters in this sample have core radii smaller than 100 kpc, which is close to the limit that our data allow us to resolve, and possibly consistent with cusped profiles.
- The remaining clusters span a broad range of core radii up to  $\sim 1500$  kpc. While a few of these clusters are likely to be disturbed systems, we find several objects with regular morphology which seem to possess a well resolved core radius.
- More than 80 per cent of this compact cluster sample has ellipticity greater than 0.2, with an average ellipticity of  $\sim 0.5$ .
- The comparison of the cluster position angles obtained within 1.5 and 3 Mpc are in very good agreement, thus confirming the absence of large substructures, and the lack of significant twisting of the cluster isopleths. We confirm the strong alignment between the cluster position angle and the major axis of the brightest ellipticals close to the cluster centre.
- We find an average power-law slope of the cluster profiles  $\beta \sim 0.8$ . This result could be compatible with flat universe models either with zero (standard CDM) or non-zero cosmological constant.
- We find evidence that the core radius is correlated, albeit with large scatter, with the cluster richness, if the entire cluster population is taken into account. On the other hand, we do not find any significant correlation between cluster ellipticity and richness, although a mild trend cannot be excluded with our data.

Future work will allow to confirm and extend our results, using the procedure developed in the present study, to estimate morphological parameters for the larger cluster sample now available in the DPOSS catalogs. Furthermore, it would be desirable to apply the same procedure to galaxy clusters extracted from cosmological simulations and compare the results with real clusters, to derive more accurate information about the cosmological parameters and the process through which galaxy clusters are assembled.

## ACKNOWLEDGMENTS

The authors wish to thank Andrea Biviano, together with Christophe Adami, for kindly providing us with his code at the beginning of this study, and for several helpful suggestions on its use. We also thank Elisabetta De Filippis for many useful discussions. VS acknowledges helpful discussions with Gabriella De Lucia, Maurilio Pannella and Paola Popesso. We thank the referee for very helpful and constructive comments. VS warmly thanks Massimo Capaccioli for assistance and hospitality at the Osservatorio Astronomico di Capodimonte, and is grateful to Ralf Bender and all his group for hospitality at MPE during part of this work. This work was partly funded by the Italian Ministry of Research through a COFIN grant and by the European Social Fund (FSE) through a Ph.D. grant. Processing and cataloging of DPOSS was supported by a generous grant from the Norris Foundation, and by

other private donors. This research has made use of the X-Rays Clusters Database (BAX) which is operated by the Laboratoire d'Astrophysique de Toulouse-Toulouse (LATT), under contract with the Centre National d'Etudes Spatiales (CNES).

## REFERENCES

- Abell, 1958, ApJS, 3, 211  
 Adami, C., Mazure, A., Katgert, P., Biviano, A., 1998, A&A, 336, 63 (AMKB98)  
 Adami, C., Mazure, A., Ulmer, M.P., Savine, C., 2001, A&A, 371, 11 (AMUS01)  
 Baier, F., 1979, Astron. Nachr., 300, 85  
 Beers, T.C., Geller, M.J., Huchra, J.P., 1982, ApJ, 257, 23  
 Beers, T.C., Tonry, J.L., 1986, ApJ, 300, 557  
 Bird, C.M., 1994, AJ, 107, 1637  
 Biviano, A., Girardi, M., 2003, ApJ, 585, 205  
 Buote, D.A., Tsai, J.C., 1996, ApJ, 458, 27  
 Carlberg, R.G., Yee, H.K.C., Ellingson, E. et al., 1997, ApJ, 485L, 13  
 Carlberg, R.G., Yee, H.K.C., Ellingson, E., 1997, ApJ, 478, 462  
 Cash, W., 1979, ApJ, 228, 939  
 Chandra X-ray Center, 2001, <http://cxc.harvard.edu/ciao/>  
 Crone, M.M., Evrard, A.E., 1994, ApJ, 434, 402  
 de Blok, W.J.G., Bosma, A., 2002, A&A, 385, 816  
 de Theije, P.A.M., Katgert, P., van Kampen, E., 1995, MNRAS, 273, 30  
 de Theije, P.A.M., Katgert, P., 1999, A&A, 341, 371-384  
 Djorgovski, S.G., Gal, R.R., Odewahn, S.C., de Carvalho, R.R., Brunner R., Longo, G., Scaramella, R., 1999, in *Wide Field Surveys in Cosmology*, eds. S. Colombi, Y. Mellier, & B. Raban, Gif sur Yvette: Editions Frontières, p. 89  
 Dressler, A., Shectman, S.A., 1988, AJ, 95, 985  
 Evrard, A.E., Mohr, J.J., Fabricant, D.G., Geller, M.J., 1993, ApJ, 419L, 9  
 Fuller, T.M., West, M.J., Bridges, T.J., 1999, ApJ, 519, 22  
 Gal, R. R., de Carvalho, R. R., Lopes, P. A. A., Djorgovski, S. G., Brunner, R. J., Mahabal, A., and S. C. Odewahn, 2003, AJ, 125, 2064  
 Garilli, B., Maccagni, D., Andreon, S., 1999, A&A, 342, 408  
 Geller, M.J., Beers, T.C., 1982, PASP, 94, 421  
 Geller, M.J., Diaferio, A., Kurtz, M.J., 1999, ApJ, 517L, 23  
 Girardi, M., Biviano, A., Giuricin, G., Mardirossian, F., Mezzetti, M., 1995, ApJ, 438, 527 (G95)  
 Girardi, M., Mezzetti, M., 2001, ApJ, 548, 79  
 Jing, Y.P., Mo, H.J., Börner, G., Fang, L.Z., 1995, MNRAS, 276, 417  
 Katgert, P., Biviano, A., Mazure, A., 2004, ApJ, 600, 657  
 Kim, R.S.J., Sloan Digital Sky Survey Collaboration, 2001, AAS, 19914202  
 Knebe, A., Muller, V., 2000, A&A, 354, 761  
 Krempec-Krygier, J., Krygier, B., 1995, A&A, 296, 359  
 Lambas, D.G., Groth, E.J., Peebles, P.J.E., AJ, 95, 996  
 Lewis, A.D., Buote, D.A., Stocke, J.T., 2003, ApJ, 586, 135  
 Majerowicz, S., Neumann, D.M., Reiprich, T.H., 2002, A&A, 394, 77  
 Markevitch, M., Vikhlinin, A., Forman, W.R., Sarazin, C.L., 1999, ApJ, 527, 545  
 Merritt, D., Tremblay, B., 1994, AJ, 108, 514  
 Miralda-Escude, J., 1995, ApJ, 438, 514  
 Moore, B., Quinn, T., Governato, F., Stadel, J., Lake, G., 1999, MNRAS, 310, 1147  
 Navarro, J.F., Frenk, C.S., White, S.D.M., 1995, MNRAS, 275, 720  
 Navarro, J.F., Frenk, C.S., White, S.D.M., 1996, ApJ, 462, 563  
 Navarro, J.F., Frenk, C.S., White, S.D.M., 1997, ApJ, 490, 493  
 Paolillo, M., Andreon, S., Longo, G., Puddu, E., Gal, R.R., Scaramella, R., Djorgovski, S.G., de Carvalho, R., 2001, A&A, 367, 59  
 Pinkney, J., Roettiger, K., Burns, J.O., Bird, C.M., 1996, ApJS, 104, 1  
 Piranomonte S., Paolillo M., Longo G., Andreon S., Puddu E., Scaramella R., Gal R., Djorgovski S.G., 2001, ASP Conf. Proc., Vol. 225, p.73  
 P. Popesso, H. Boehringer, J. Brinkmann, W. Voges, D. G. York, 2004, A&A, in press  
 Postman, M., Geller, M.J., Huchra, J.P., 1988, AJ, 95, 267  
 Sand, D.J., Treu, T., Ellis, R.S., 2002, ApJ, 574L, 129  
 Sarazin, C.L., 1980, ApJ, 236, 75  
 Shapiro, P.R., Iliev, I.T., 2000, ApJ, 542L, 1  
 Sherpa Reference Manual, 2001, Chandra X-ray Center, Smithsonian Astrophysical Observatory, [http://cxc.harvard.edu/ciao/download/doc/sherpa.html\\_manual/index.html](http://cxc.harvard.edu/ciao/download/doc/sherpa.html_manual/index.html)  
 Solanes, J.M., Salvador-Solè, E., González-Casado, G., 1999, A&A, 343, 733  
 Struble, M.F., Ftaclas, C., 1994, AJ, 108, 1  
 Struble, M.F., Rood, H.J., 1999, ApJS, 125, 35  
 Swaters, R.A., Madore, B.F., Trehella, M., 2000, ApJ, 531, L107  
 Walter, C., Klypin, A., 1996, ApJ, 462, 13  
 Weir, N., Fayyad, U., Djorgovski, S.G., Roden, J., 1995, PASP, 107, 1243  
 West, M.J., Bothun, G.D., 1990, ApJ, 350, 36  
 West, M.J., Oemler, A., Dekel, A., 1988, ApJ, 327, 1  
 Wu, X., Chiueh, T., 2001, ApJ, 547, 82  
 Zhou, X., Arimoto, N., Tanaka, I., Jiang, Z., Chen, J., 2003, PASJ, 55, 891

**Table 1.** The compact cluster sample. The second and third columns give the cluster coordinates (from the Abell catalogue) at equinox J2000.0. In columns 4, 5, 6, and 7 we give, respectively, the cluster spectroscopic redshift derived from literature (in parentheses, the number  $N_z$  of galaxies used to measure  $z$ ; see Struble & Rood (1999) for discussion on lower limits), the Abell richness class (Abell 1958), the X-ray luminosity in the 0.1-2.4 keV band (from the BAX database - LATT), and the plate of the POSS archive where the cluster is imaged.

Abell N.	RA	Dec	$z (N_z)$	Abell Richness Class	$L_X (10^{44} \text{ erg/s})$	Plate
28	0:25:10	8:08:34	0.184 (-)	2	-	680
41	0:28:46	7:51:36	0.275 (3)	3	-	752
79	0:40:37	18:08:27	0.093 (1)	1	-	540
84	0:41:50	21:24:25	0.103 (>1)	1	1.82	540
98	0:46:26	20:29:24	0.104 (24)	3	0.94	540
171	1:16:46	16:15:46	0.070 (>4)	0	-	611
175	1:19:33	14:52:44	0.129 (>0)	2	-	611
192	1:24:17	4:29:38	0.121 (-)	2	0.84	755
286	1:58:26	-1:46:26	0.160 (-)	2	2.53	829
566	7:04:29	63:17:31	0.098 (9)	2	2.81	088
655	8:25:20	47:08:13	0.124 (1)	3	4.90	210
763	9:12:28	16:00:36	0.085 (5)	1	2.27	634
910	10:02:59	67:10:30	0.206 (2)	4	5.43	091
971	10:19:46	40:58:55	0.06 (?)	1	1.10	317
1661	13:01:48	29:04:51	0.167 (4)	2	0.65	443
1672	13:04:45	33:33:57	0.188 (1)	1	4.25	382
1677	13:05:52	30:53:56	0.184 (1)	2	5.37	443
1835	14:01:01	2:51:32	0.252 (>1)	0	29.80	793
1902	14:21:46	37:18:21	0.16 (1)	2	4.55	326
1914	14:26:02	37:49:33	0.171 (2)	2	17.30	326
2061	15:21:15	30:39:18	0.077 (20)	1	4.85	449
2065	15:22:42	27:43:22	0.072 (22)	2	5.55	449
2069	15:23:57	29:54:25	0.116 (9)	2	3.45	449
2083	15:29:26	30:44:45	0.114 (1)	1	-	449
2142	15:58:16	27:13:30	0.091 (103)	2	21.24	516
2177	16:20:58	25:44:56	0.161 (>0)	0	2.20	517
2178	16:21:30	24:39:00	0.093 (2)	1	0.28	517
2223	16:42:30	27:26:24	0.103 (-)	0	-	517

**Table 2.** Parameter estimates for the compact clusters. Column 1: cluster identification; columns 2-6: estimated parameters: core radius,  $\beta$  power law index, ellipticity, major axis position angle and projected central density. The errors are  $1\sigma$  levels derived as discussed in the text. The tabulated  $\Sigma_0$  are not corrected for the different absolute completeness limits of the clusters.

Abell N.	$r_{core}$ (kpc)	$\beta$	$\epsilon$	$\theta$ (rad)	$\Sigma_0^*$ $10^{-5}\text{gal./kpc}^2$
28	$370^{+260}_{-150}$	$1.2^{+0.5}_{-0.3}$	$0.61^{+0.06}_{-0.07}$	$0.06^{+0.17}_{-0.15}$	$9^{+6}_{-3}$
41	$1000^{+2200}_{-370}$	$1.6^{+6}_{-0.5}$	$0.71^{+0.05}_{-0.05}$	$1.27^{+0.07}_{-0.07}$	$4.6^{+1.8}_{-1.4}$
79	$140^{+96}_{-89}$	$0.83^{+0.2}_{-0.15}$	$0.55^{+0.09}_{-0.1}$	$1.78^{+0.16}_{-0.2}$	$25^{+40}_{-9}$
84	$360^{+210}_{-140}$	$0.96^{+0.2}_{-0.16}$	$0.47^{+0.08}_{-0.09}$	$2.21^{+0.2}_{-0.19}$	$12^{+7}_{-4}$
98	$970^{+490}_{-300}$	$0.97^{+0.3}_{-0.18}$	$0.52^{+0.04}_{-0.04}$	$2.94^{+0.09}_{-0.09}$	$8.1^{+2}_{-1.7}$
171	$160^{+94}_{-63}$	$1.00^{+0.3}_{-0.16}$	$0.25^{+0.13}_{-0.14}$	$1.9^{+0.8}_{-0.5}$	$27^{+15}_{-9}$
175	$390^{+210}_{-160}$	$0.70^{+0.13}_{-0.09}$	$0.58^{+0.05}_{-0.05}$	$2.34^{+0.12}_{-0.11}$	$9^{+5}_{-2}$
192	$33^{+57}_{-30}$	$0.79^{+0.15}_{-0.1}$	$0.73^{+0.07}_{-0.07}$	$2.71^{+0.14}_{-0.17}$	$134^{+\infty}_{-80}$
286	$310^{+210}_{-120}$	$0.94^{+0.3}_{-0.14}$	$0.36^{+0.09}_{-0.09}$	$3.1^{+0.2}_{-0.2}$	$11^{+6}_{-4}$
566	$100^{+69}_{-67}$	$0.44^{+0.04}_{-0.04}$	$0.17^{+0.08}_{-0.09}$	$2.3^{+0.5}_{-0.6}$	$19^{+20}_{-6}$
655	$1300^{+550}_{-410}$	$1.3^{+0.5}_{-0.3}$	$0.34^{+0.04}_{-0.04}$	$1.62^{+0.12}_{-0.12}$	$6.8^{+1.5}_{-1}$
763	$30^{+35}_{-29}$	$0.61^{+0.07}_{-0.07}$	$0.54^{+0.09}_{-0.09}$	$0.9^{+0.2}_{-0.2}$	$84^{+\infty}_{-50}$
910	$1400^{+2600}_{-520}$	$1.0^{+1.8}_{-0.2}$	$0.44^{+0.06}_{-0.07}$	$2.97^{+0.17}_{-0.18}$	$1.9^{+0.5}_{-0.6}$
971	$39^{+34}_{-37}$	$0.46^{+0.04}_{-0.03}$	$0.70^{+0.03}_{-0.03}$	$1.50^{+0.07}_{-0.07}$	$91^{+\infty}_{-40}$
1661	$890^{+770}_{-400}$	$1.1^{+0.8}_{-0.3}$	$0.64^{+0.05}_{-0.06}$	$1.29^{+0.10}_{-0.10}$	$4.2^{+2}_{-1.3}$
1672	$280^{+270}_{-150}$	$0.74^{+0.3}_{-0.15}$	$0.006^{+0.19}_{-0.006}$	$2.4^{+4}_{-2.4}$	$3.4^{+3}_{-1.3}$
1677	$15^{+24}_{-14}$	$0.57^{+0.07}_{-0.07}$	$0.43^{+0.12}_{-0.14}$	$2.6^{+0.3}_{-0.4}$	$73^{+\infty}_{-50}$
1835	$81^{+130}_{-58}$	$0.54^{+0.07}_{-0.07}$	$0.56^{+0.06}_{-0.07}$	$2.58^{+0.15}_{-0.16}$	$19^{+\infty}_{-10}$
1902	$380^{+250}_{-170}$	$0.66^{+0.16}_{-0.11}$	$0.1^{+0.16}_{-0.1}$	$2.5^{+0.6}_{-2}$	$4.6^{+2}_{-1.3}$
1914	$140^{+88}_{-80}$	$0.63^{+0.07}_{-0.08}$	$0.50^{+0.06}_{-0.07}$	$0.99^{+0.15}_{-0.15}$	$18^{+20}_{-7}$
2061	$780^{+260}_{-300}$	$0.87^{+0.16}_{-0.16}$	$0.70^{+0.03}_{-0.03}$	$0.78^{+0.06}_{-0.06}$	$10.7^{+4}_{-1.9}$
2065	$97^{+48}_{-51}$	$0.60^{+0.05}_{-0.05}$	$0.17^{+0.08}_{-0.08}$	$2.8^{+0.3}_{-0.5}$	$48^{+40}_{-14}$
2069	$340^{+190}_{-150}$	$0.82^{+0.19}_{-0.15}$	$0.35^{+0.08}_{-0.09}$	$2.7^{+0.3}_{-0.3}$	$9^{+5}_{-3}$
2083	$23^{+20}_{-18}$	$0.64^{+0.05}_{-0.06}$	$0.47^{+0.08}_{-0.08}$	$1.4^{+0.2}_{-0.2}$	$140^{+\infty}_{-70}$
2142	$857^{+300}_{-310}$	$0.79^{+0.15}_{-0.14}$	$0.54^{+0.03}_{-0.04}$	$2.46^{+0.1}_{-0.09}$	$8.5^{+3}_{-1.4}$
2177	$55^{+130}_{-50}$	$0.53^{+0.08}_{-0.08}$	$0.72^{+0.06}_{-0.07}$	$1.93^{+0.15}_{-0.13}$	$25^{+\infty}_{-16}$
2178	$340^{+440}_{-130}$	$0.86^{+0.5}_{-0.14}$	$0.40^{+0.1}_{-0.11}$	$1.4^{+0.2}_{-0.2}$	$11^{+5}_{-4}$
2223	$37^{+53}_{-29}$	$0.60^{+0.06}_{-0.06}$	$0.60^{+0.06}_{-0.07}$	$1.15^{+0.13}_{-0.13}$	$78^{+\infty}_{-40}$

**Table 3.** Parameter estimates for the compact clusters. Column 1: cluster identification; columns 2-3: richness estimates ( $R_A$ ,  $R_{LF}$ ) obtained as described in the text; column 4: total number of galaxies used for profile fitting in the  $6 \times 6 \text{ Mpc}^2$  region; column 5: background density as estimated in the external annulus ( $4 \leq r \leq 5 \text{ Mpc}$ ); column 6: background density as estimated with a simultaneous fit on all 8 parameters; column 7: Kolmogorov Smirnov confidence levels for the distribution of the cluster galaxy position angles. The errors are  $1\sigma$  levels.

Abell N.	$R_A$ (gal.)	$R_{LF}$ (gal.)	$N(6 \times 6 \text{ Mpc}^2)$ (gal.)	$\Sigma_{bkg}$ gal/squaremin	$\Sigma_{bkg}^{fit}$ gal/squaremin	$P_{KS}(d > d_{obs})$
28	39	69	306	$0.36 \pm 0.03$	0.33	0.8
41	35	216	189	$0.33 \pm 0.04$	0.35	0.3
79	28	38	632	$0.34 \pm 0.02$	0.30	0.4
84	36	81	678	$0.42 \pm 0.02$	0.37	0.5
98	50	326	853	$0.31 \pm 0.02$	0.30	0.4
171	23	46	939	$0.30 \pm 0.01$	0.30	0.2
175	39	86	532	$0.28 \pm 0.02$	0.28	0.5
192	33	80	337	$0.28 \pm 0.02$	0.24	0.7
286	26	140	327	$0.29 \pm 0.02$	0.31	0.7
566	57	108	834	$0.36 \pm 0.02$	0.38	0.3
655	65	329	630	$0.31 \pm 0.03$	0.28	0.4
763	10	79	818	$0.33 \pm 0.01$	0.32	0.04
910	49	164	232	$0.25 \pm 0.03$	0.17	0.2
971	38	74	1641	$0.35 \pm 0.01$	0.34	0.05
1661	39	104	326	$0.30 \pm 0.02$	0.31	0.02
1672	30	76	217	$0.26 \pm 0.02$	0.23	0.5
1677	30	125	245	$0.22 \pm 0.02$	0.22	0.1
1835	64	214	274	$0.25 \pm 0.03$	0.23	0.02
1902	39	183	366	$0.26 \pm 0.02$	0.26	0.3
1914	43	171	370	$0.31 \pm 0.02$	0.31	0.3
2061	37	231	056	$0.33 \pm 0.01$	0.33	0.4
2065	67	228	583	$0.34 \pm 0.01$	0.35	0.005
2069	22	162	625	$0.38 \pm 0.02$	0.37	0.02
2083	21	93	513	$0.29 \pm 0.02$	0.28	0.2
2142	59	194	841	$0.34 \pm 0.02$	0.28	$9 \times 10^{-6}$
2177	27	95	468	$0.53 \pm 0.03$	0.48	0.3
2178	19	83	908	$0.47 \pm 0.02$	0.45	0.002
2223	21	73	635	$0.36 \pm 0.03$	0.36	0.004

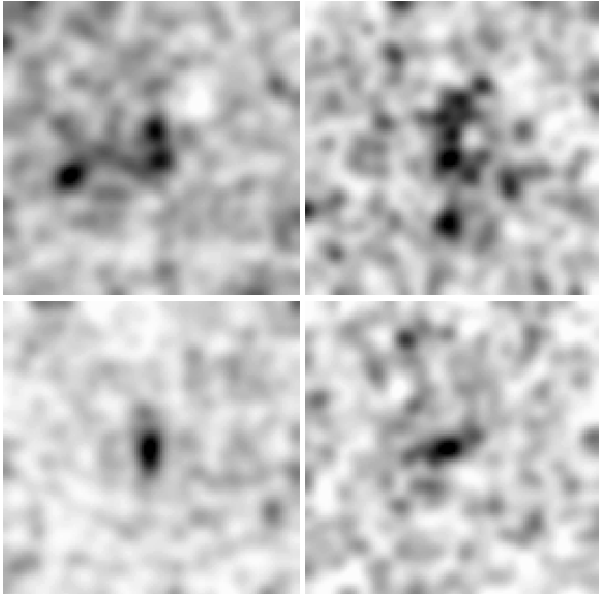


**Figure 1.** Typical examples of cluster galaxy number density maps, after smoothing with a Gaussian filter with  $\sigma = 250$  kpc (in the cluster rest-frame). The upper panels show two typical subclustered systems (A1035 and A1081) which are rejected by our selection criteria, while the lower panels present two compact clusters (A286 and A1661) which are included in our sample. Each map covers an area of  $10 \times 10 \text{ Mpc}^2$ .

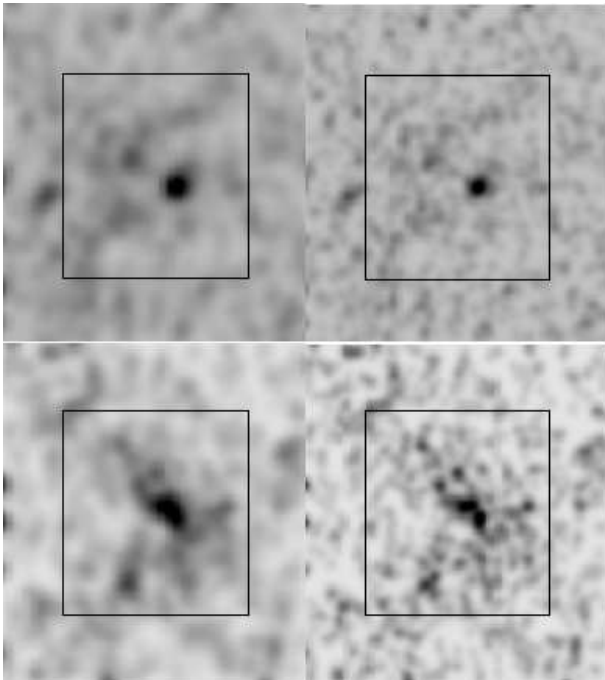


**Figure 2.** Smoothed maps for A2083 (top) and A175 (bottom). Smoothing is gaussian with  $\sigma = 250$  kpc (left) and  $\sigma = 150$  kpc (right). The lower right panel shows cluster substructure on scales of order 150 kpc. The whole frame is  $10 \times 10 \text{ Mpc}^2$  wide, while the inner square is  $6 \times 6 \text{ Mpc}^2$ .

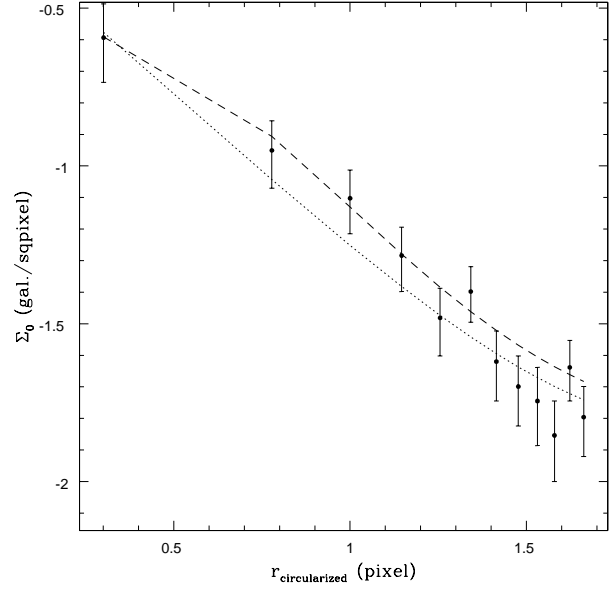


**Figure 3.** Example of a unidimensional fit on binned data for one cluster of the sample (A286), with both a cusped profile (dotted line) and a  $\beta$ -model (dashed line).

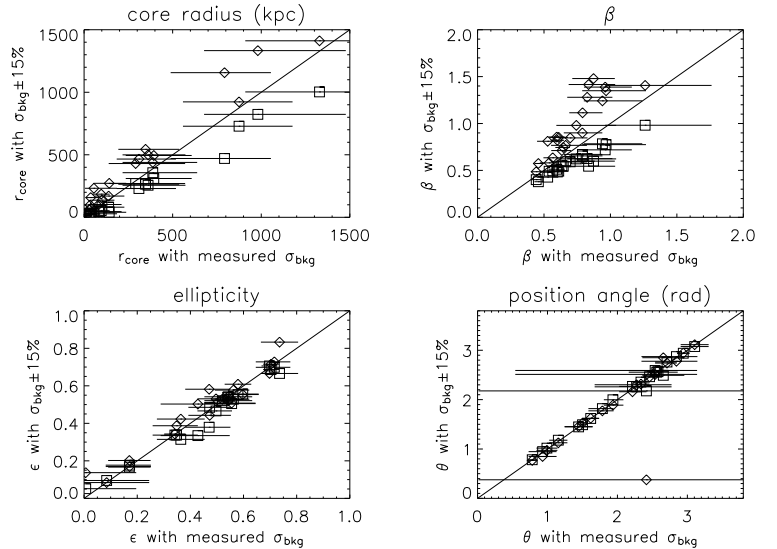


**Figure 4.** Effect of a 15% background misestimate on the parameters: core radius (top left),  $\beta$  (top right), ellipticity (bottom left) and position angle (bottom right). In all the panels, the diamonds mark the parameter value fitted with a background density overestimated by 15% of its measured value vs. the usual measured value, while the squares mark the parameter value fitted with an underestimated background vs. the usual value. All the fits are performed in the  $6 \times 6 \text{ Mpc}^2$  region. The solid line traces the bisector.

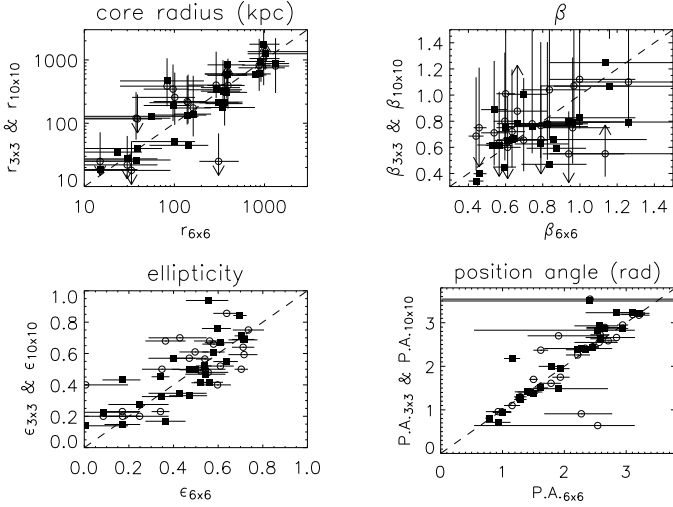


**Figure 5.** Dependence of the parameters on the fitted region: core radius (top left),  $\beta$  (top right), ellipticity (bottom left) and position angle (bottom right). In all the panels, the empty/filled symbols mark the parameter value fitted in the  $3 \times 3 Mpc^2 / 10 \times 10 Mpc^2$  regions respectively vs. the value in the  $6 \times 6 Mpc^2$  region. The dashed line traces the bisector.

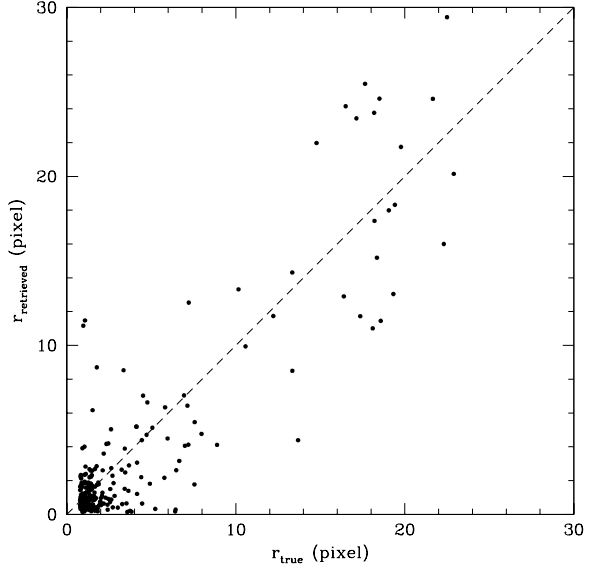


**Figure 7.** Retrieved vs. true core radius for the mock cluster sample. The dashed line traces the bisector.

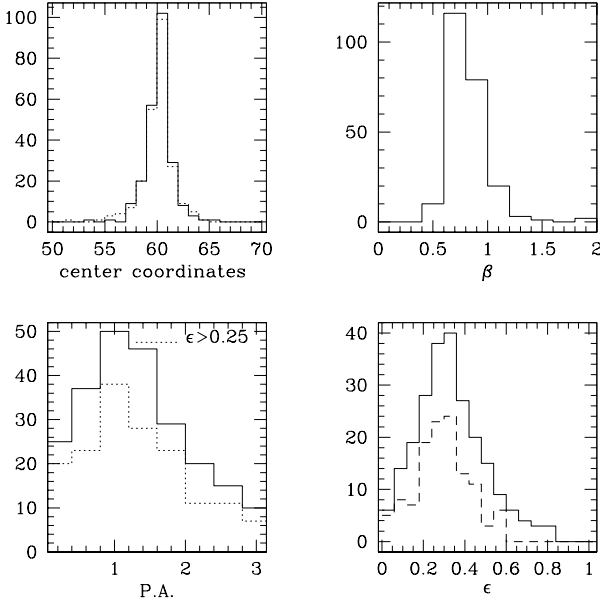


**Figure 6.** Distribution of the mock cluster parameters. Upper panels: distributions of the retrieved  $\beta$  values (right) and centre coordinates (left - solid and dotted line for  $x_0$  and  $y_0$ , input value was (60,60)). Lower right panel: distribution of retrieved ellipticity; the solid line shows the whole sample, dashed line denotes the high S/N clusters. Lower left panel: distribution of position angles, solid line is for the whole sample, dotted line is for clusters with retrieved ellipticity greater than 0.25.

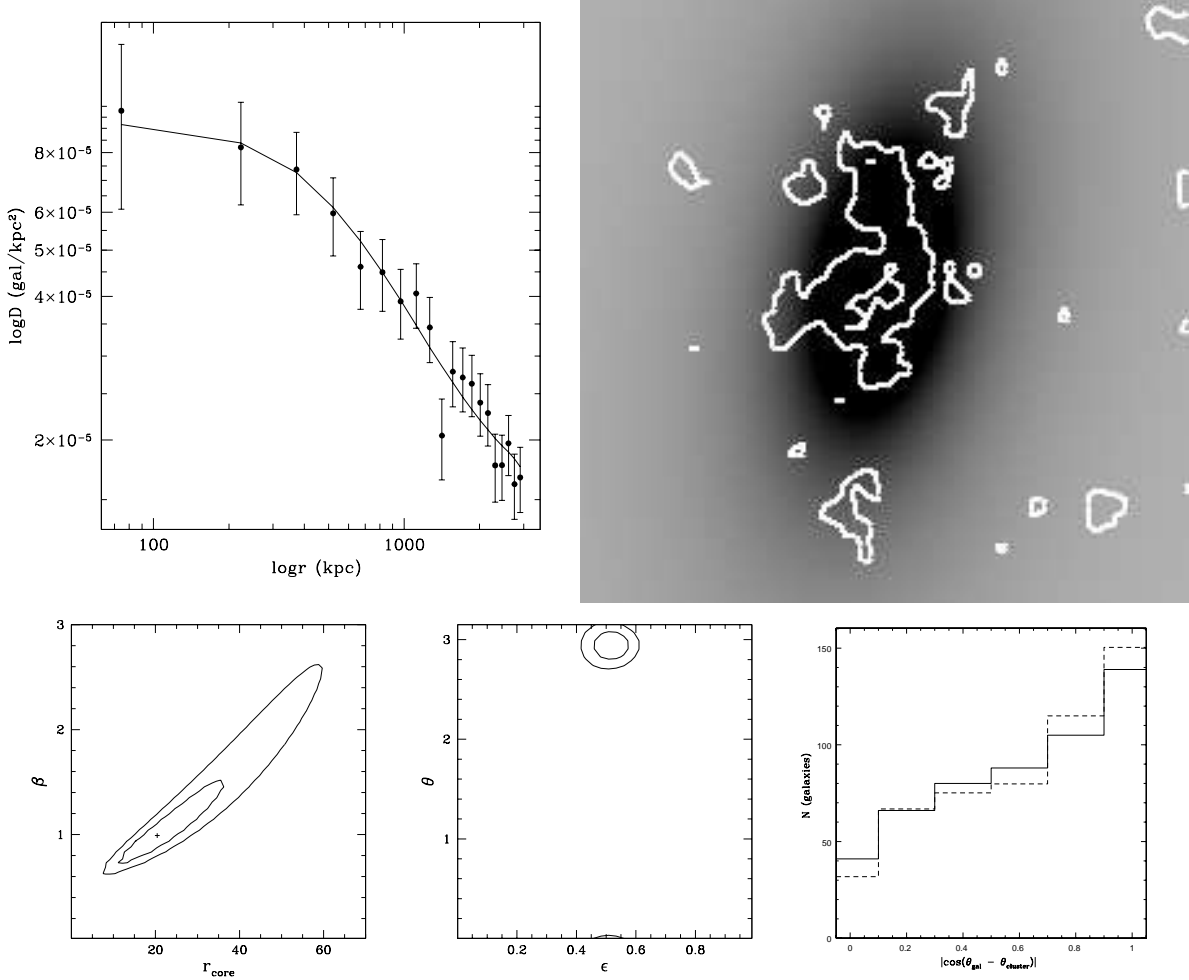


**Figure 8.** Cluster A98. Top left panel: radial profile (the solid line marks the model while dots mark the data, see text for details). Top right panel: cluster isocontours in the fitted region ( $6 \times 6 \text{ Mpc}^2$ ) plotted on the model. Bottom left and central panels: 1 and  $2\sigma$  confidence regions for the couples ( $r_{\text{core}} - \beta$ ) (with  $\Sigma_0$  free to vary) and ( $\epsilon - \theta$ ) respectively ( $r_{\text{core}}$  is in units of bins (1 bin = 0.325 arcmin  $\simeq$  50 kpc), while  $\theta$  is expressed in radians). Bottom right panel: the misalignments of galaxy P.A. with cluster P.A. (solid line) compared with those expected for a random distribution of galaxy position angles (dashed line).

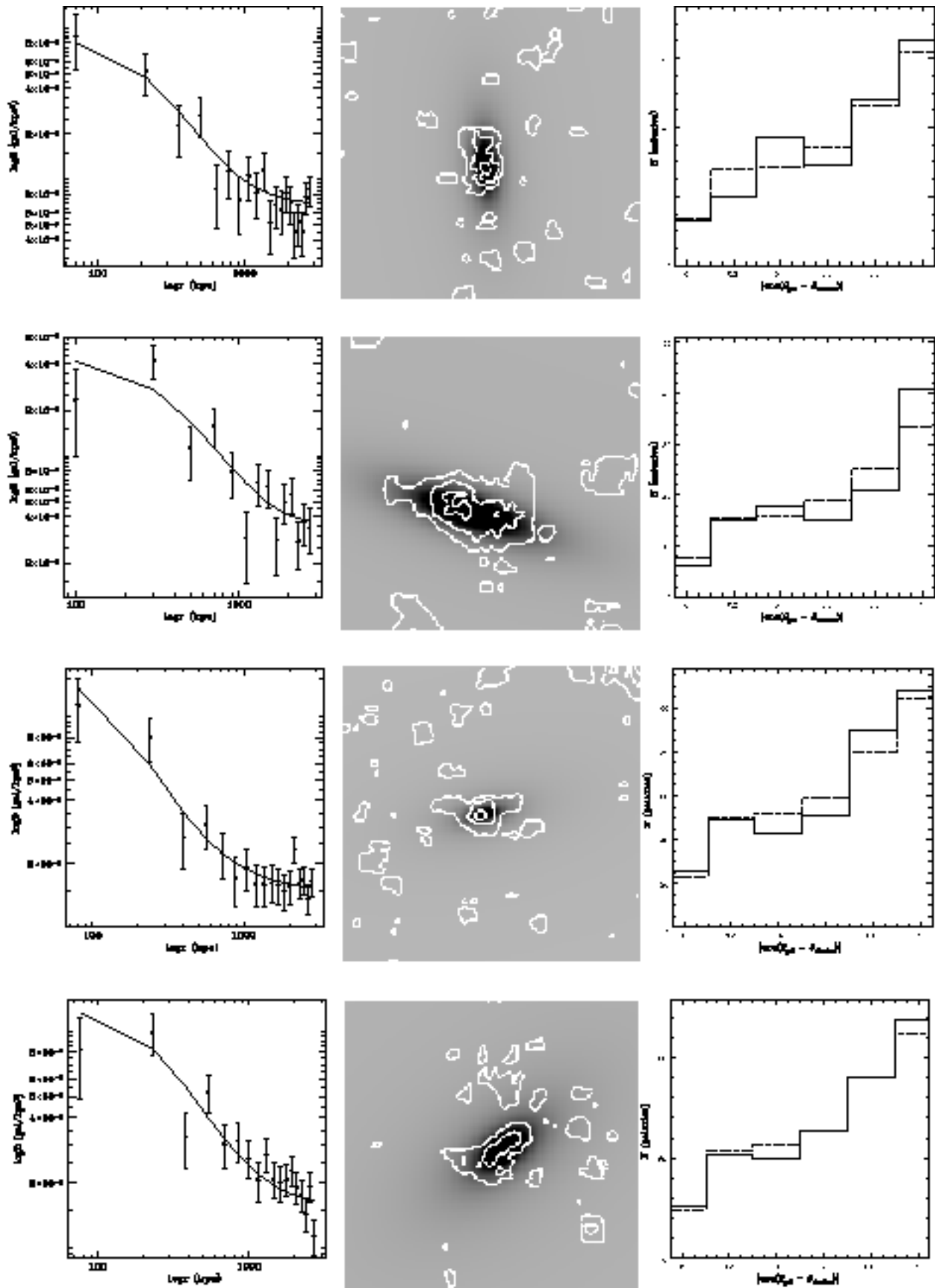


**Figure 9.** Radial profile and contour plot in the fitted region ( $6 \times 6 \text{ Mpc}^2$  - model images are all shown with the same contrast/bias) and galaxy P.A. distribution for (starting from top): A28, A41, A79, A84 (see fig. 2 for details).

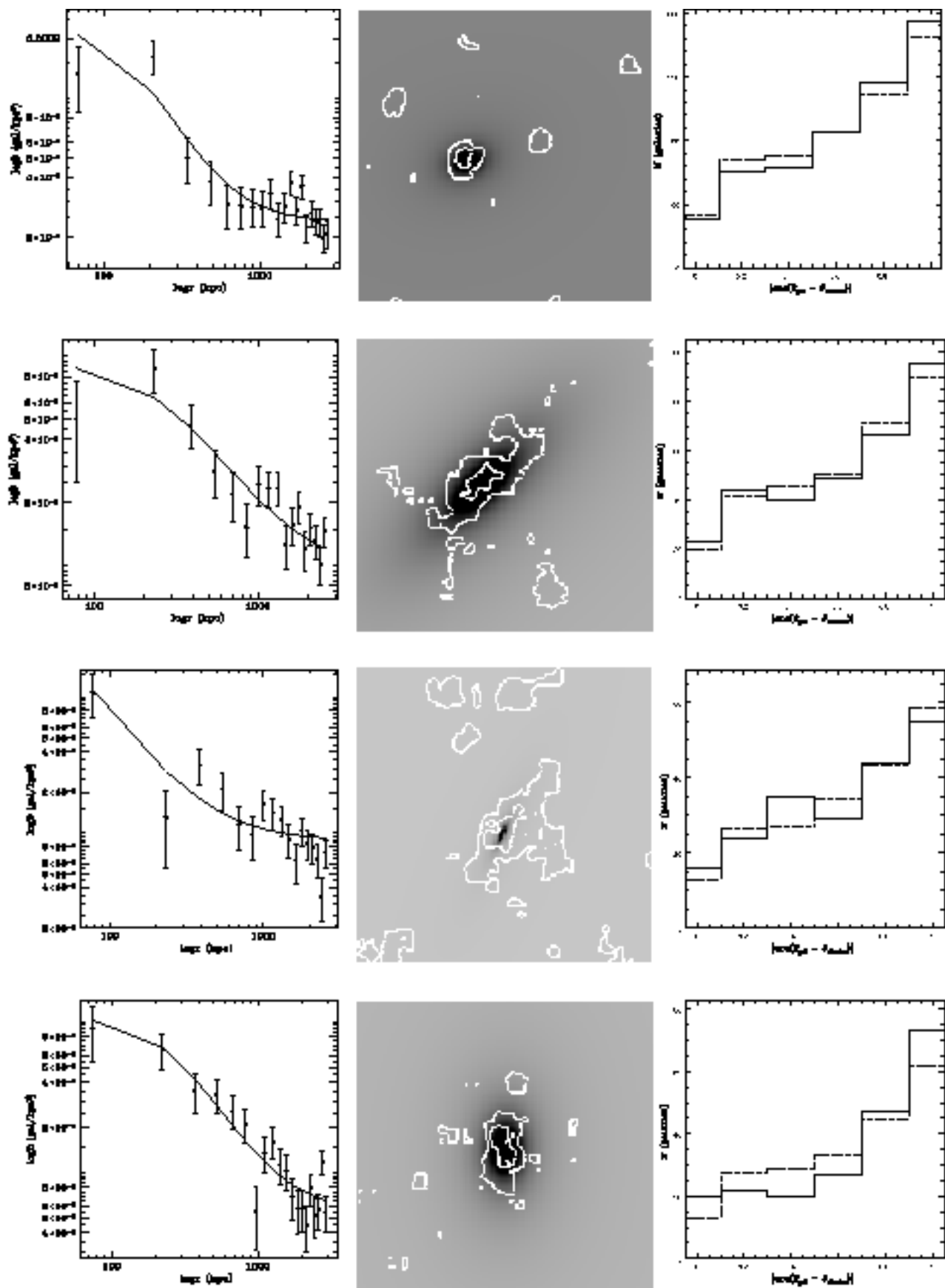


Figure 9. (continued). Starting from top: A171, A175, A192, A286.

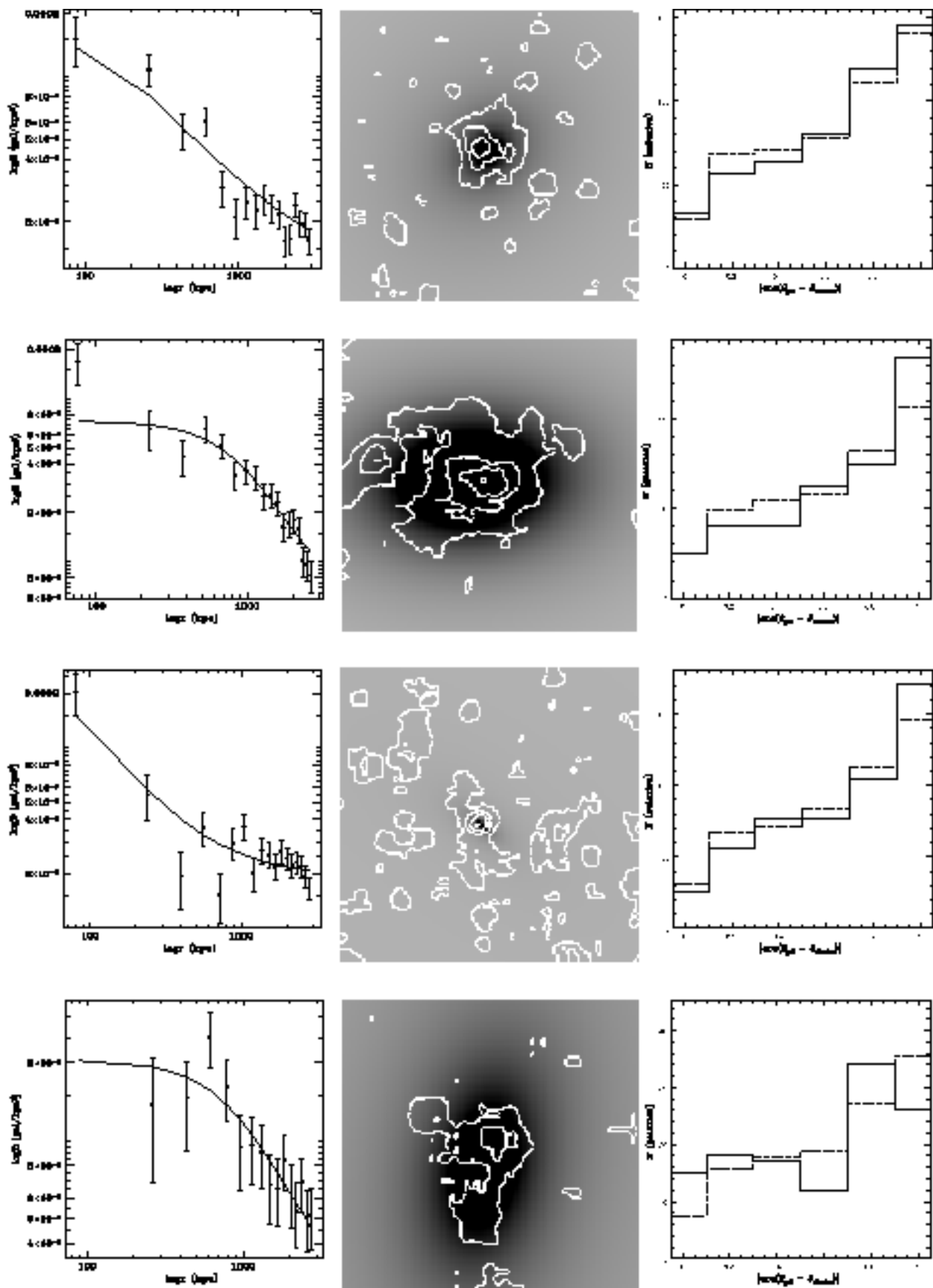


Figure 9. (continued). Starting from top: A566, A655, A763, A910.

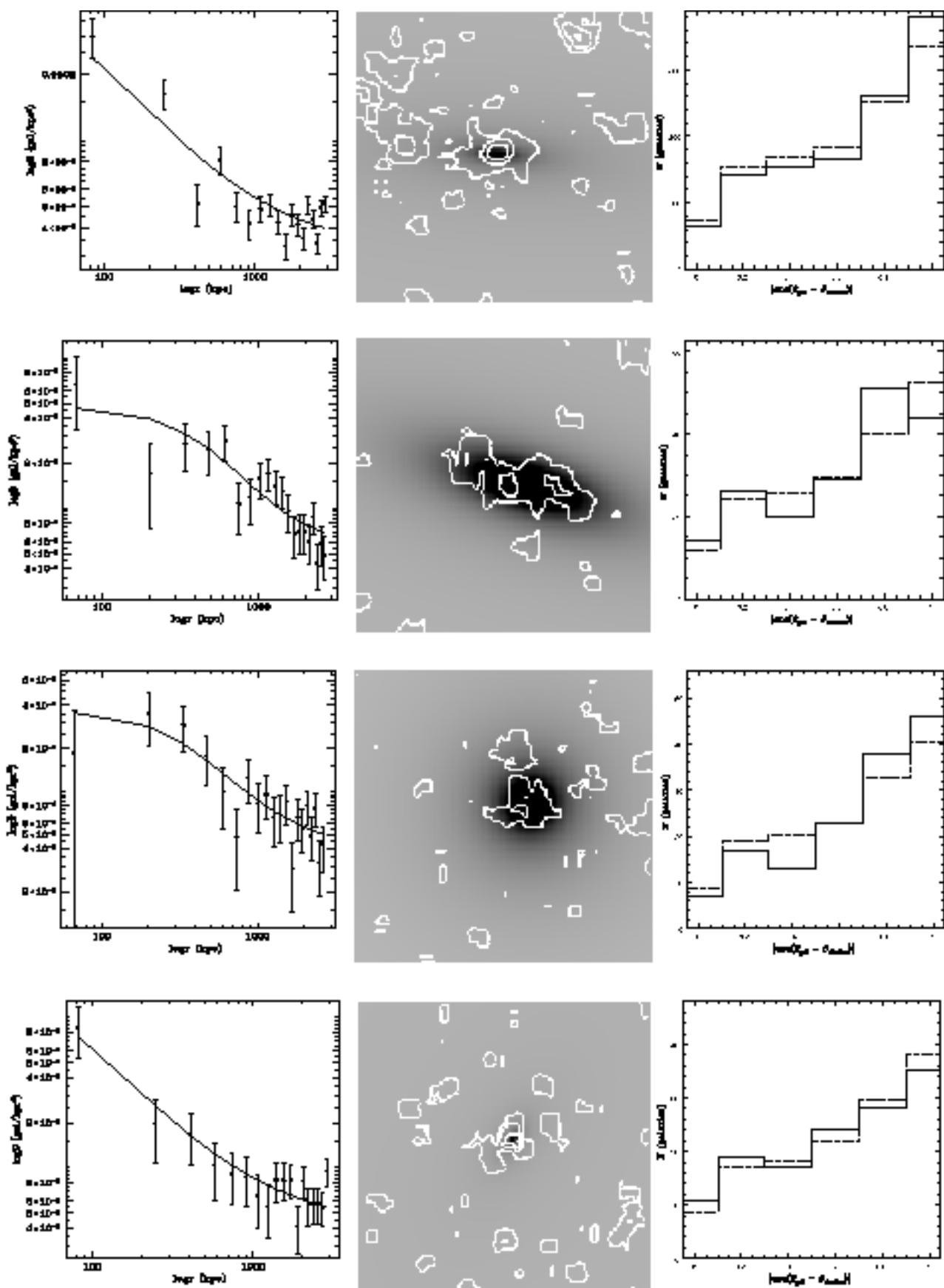


Figure 9. (continued). Starting from top: A971, A1661, A1672, A1677.

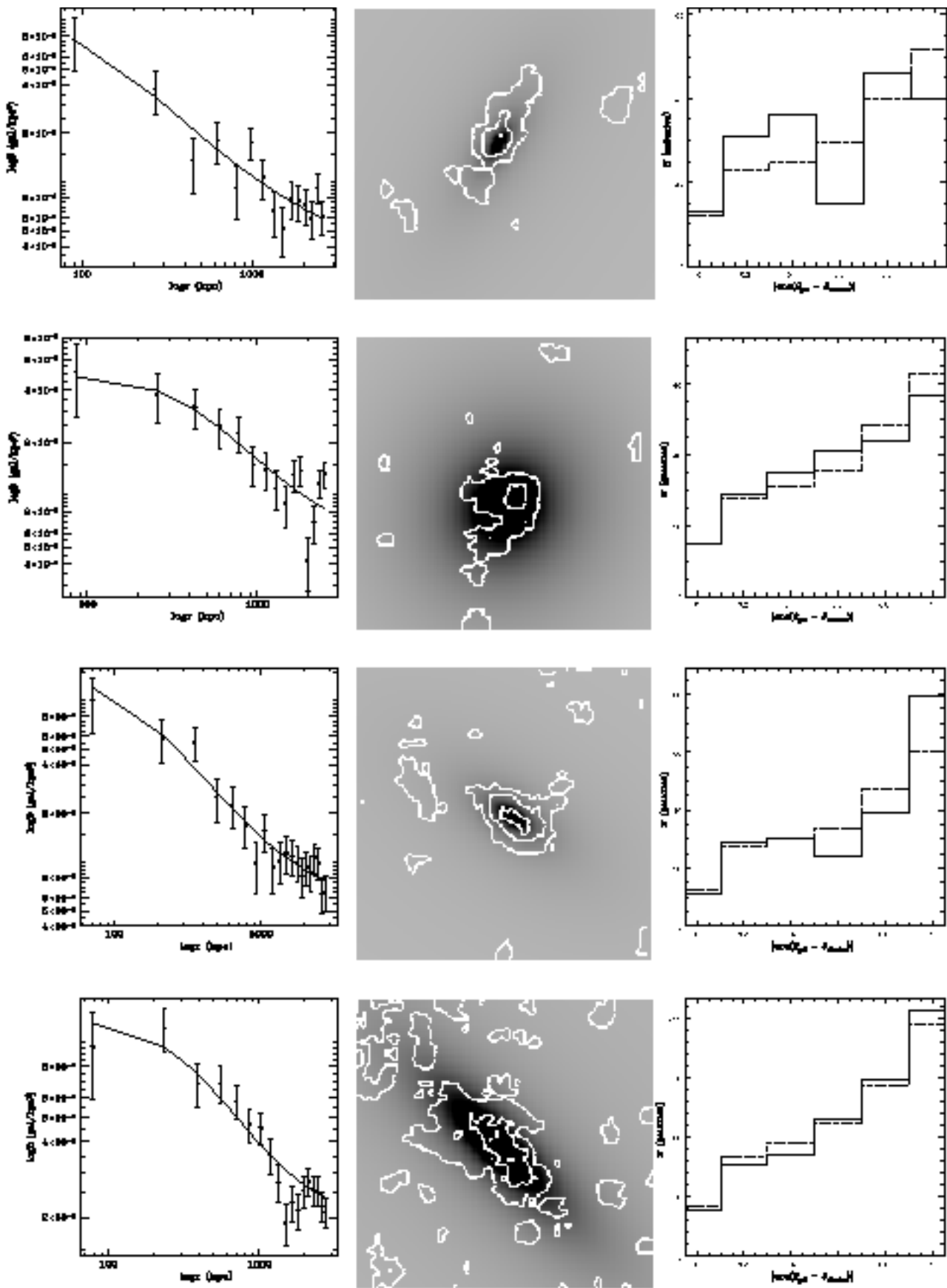


Figure 9. (continued). Starting from top: A1835, A1902, A1914, A2061.

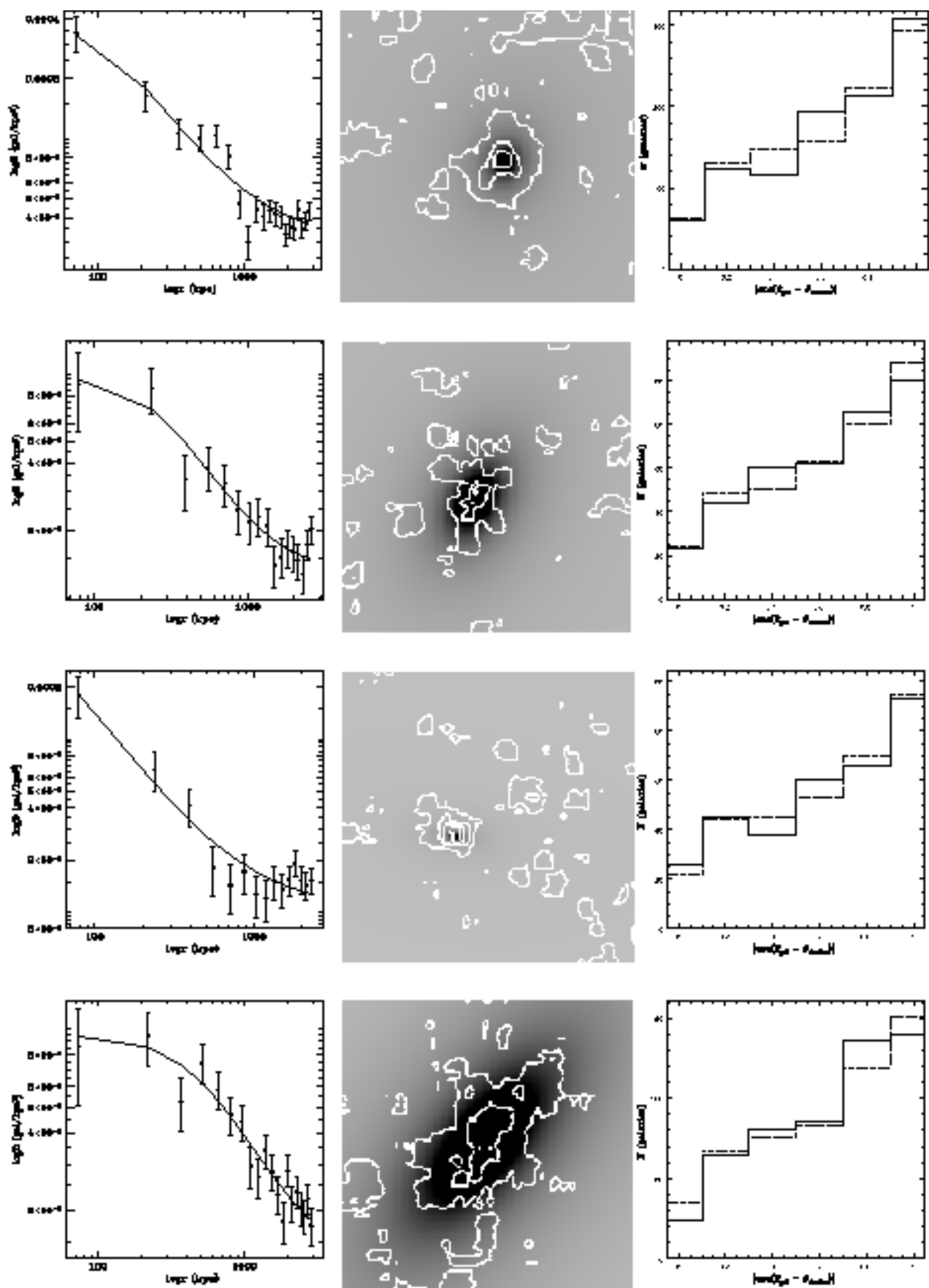


Figure 9. (continued). Starting from top: A2065, A2069, A2083, A2142.

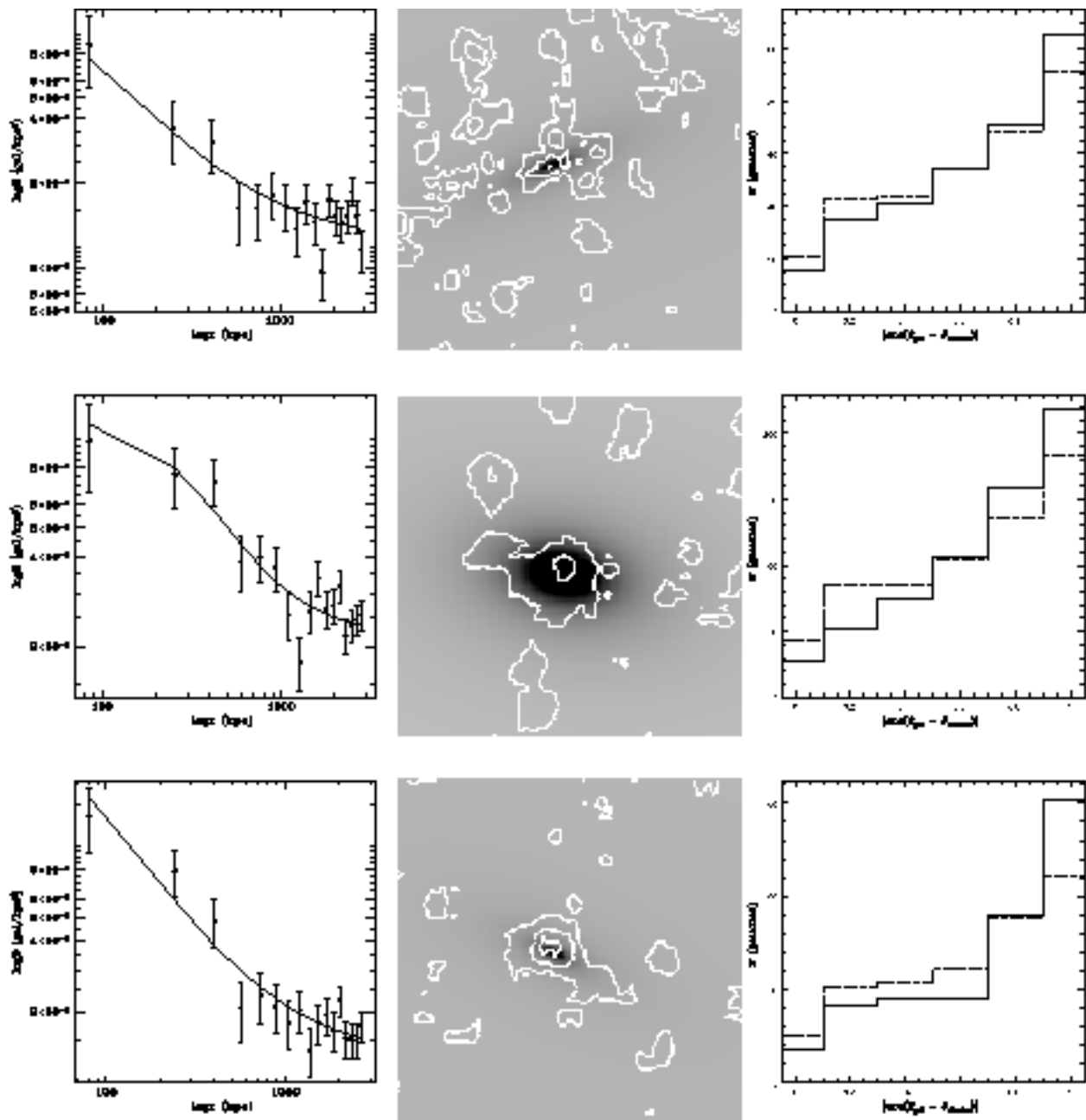
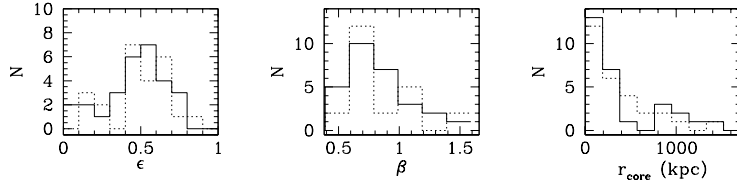
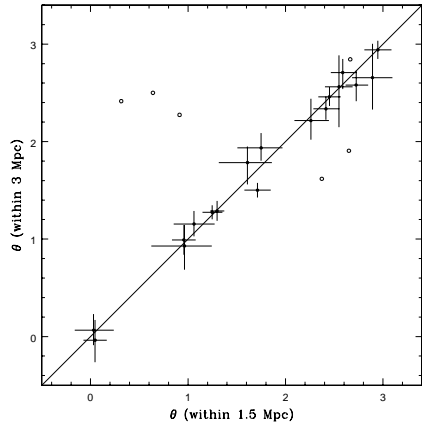


Figure 9. (continued). Starting from top: A2177, A2178, A2223.



**Figure 10.** Distributions of the  $\beta$ -model parameters for the compact cluster sample: ellipticity (left),  $\beta$  power-law index (center) and core radius (right). The solid and dashed lines show the results obtained through the fit in the  $6 \times 6 \text{ Mpc}^2$  and  $3 \times 3 \text{ Mpc}^2$  regions, respectively.



**Figure 11.** Position angles obtained for compact clusters fitting the galaxy distribution within 1.5 Mpc from the cluster centre vs. position angles within 3 Mpc from cluster centre. The open circles refer to clusters for which the position angle of the major axis is poorly determined due to the small ellipticity ( $\epsilon < 0.25$ ); the continuous line traces the bisector.

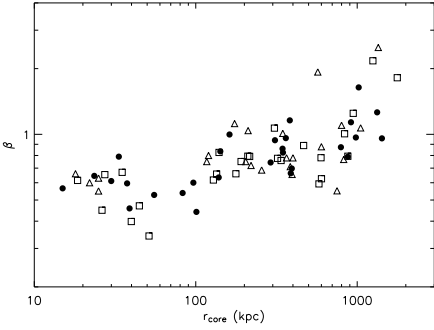


**Figure 12.** The coupling of core radius and  $\beta$  values. Different symbols show fit results in the three different regions. Solid dots mark the results from the  $6 \times 6 \text{ Mpc}^2$  region, while triangles and squares mark the results from the  $3 \times 3$  and  $10 \times 10 \text{ Mpc}^2$  regions respectively.

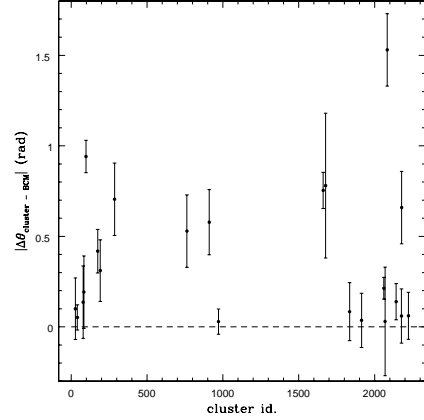


**Figure 13.** Orientation of the cluster dominant galaxies relative to the cluster major axis (clusters for which the position angle is poorly determined (see text and figure 11) are not included).

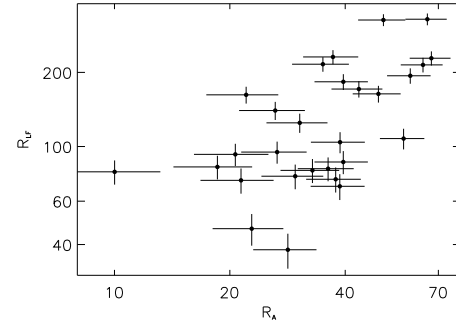


**Figure 14.** Comparison of the two richness estimates  $r_A$  (based on the Abell criterion) and  $r_{LF}$  (based on the clusters luminosity function - see text for details).

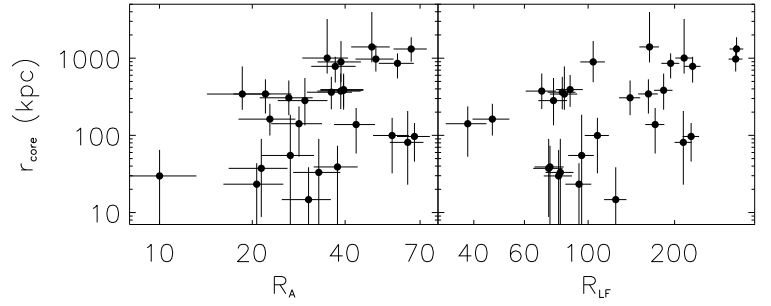


**Figure 15.** Core radius versus cluster richness, for both the Abell and luminosity function richness estimates.

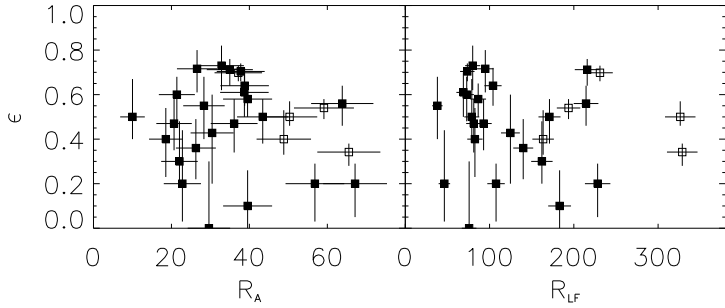


**Figure 16.** Ellipticity vs. cluster richness, for both the Abell and luminosity function richness estimates. Empty symbols mark the less regular clusters (see text for details).

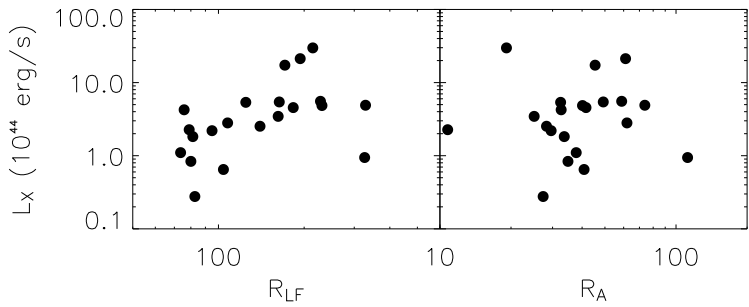


**Figure 17.** Cluster X-ray luminosity vs. richness, for both the Abell and luminosity function richness estimates. Only 21 clusters with X-ray luminosities available are shown .